UCLA

PLASMA PHYSICS GROUP

UNIVERSITY OF CALIFORNIA
LOS ANGELES

ENGINEERING | PHYSICS | METEOROLOGY

Turbulence in Electrostatic Ion Acoustic Shocks

R.W. Means, F.V. Coroniti,

A.Y. Wong and R.B. White

PPG-149 May, 1973

TURBULENCE IN ELECTROSTATIC ION ACOUSTIC SHOCKS

R. W. Means, F. V. Coroniti, A. Y. Wong, and R. B. White

Department of Physics, University of California, Los Angeles, California 90024

Abstract

Three types of collisionless electrostatic ion acoustic shocks are investigated using the University of California, Los Angeles, double plasma (DP) device: a) laminar shocks; b) small amplitude turbulent shocks in which the turbulence is confined to be upstream of the shock potential jump; c) large amplitude turbulent shocks in which the wave turbulence occurs throughout the shock transition. The wave turbulence is generated by ions which are reflected from the shock potential; linear theory spatial growth increments agree with experimental values. The experimental relationship between the shock Mach number and the shock potential is shown to be inconsistent with theoretical shock models which assume that the electrons are isothermal. Theoretical calculations which assume a trapped electron equation of a state and a turbulently flattened velocity distribution function for the reflected ions yields a Mach number vs potential relationship in agreement with experiment.

I. INTRODUCTION

Collisionless laminar electrostatic ion acoustic shocks were first predicted by Moiseev and Sagdeev.[1] They showed that the Debye length, dispersion limited solitary wave calculated using isothermal electron-cold ion fluid theory could be converted into a shock transition by the inclusion of a small fractional density of ions which are reflected by the shock potential. They suggested that these reflected ions might stimulate a counter-streaming instability thus introducing turbulent dissipation into the laminar shock structure. This theory predicted steady shock solutions only for Mach numbers below 1.6. (In the shock frame, the Mach number is defined as the upstream flow speed divided by the long wavelength linear ion acoustic speed.) For a Maxwellian distribution of upstream ions and isothermal electrons, Bardotti and Segre[2] showed that the maximum or critical Mach number decreased with decreasing electron to ion temperature ratio (T_e/T_i), and that for $T_e/T_i < 12.5$, no steady shock solutions were possible. In the cold ion limit, however, Montgomery[3] and Montgomery and Joyce[4] demonstrated that if the shock were treated as an ion acoustic Bernstein-Greene-Kruskal mode,[5] then the freedom to adjust the distribution of electrons trapped in the shock potential permitted shock-like solutions to be constructed for any Mach number. In numerical simulation experiments Forslund and Shonk[6] and Forslund and Freidberg[7] investigated high Mach number, high T_e/T_i shocks and found steady laminar shocks with Mach numbers between 3 and 6 in which the trapped electron distribution function was essentially flat. The high T_e/T_i ratios and one-dimensional property of the simulations precluded a study of reflected ion driven turbulence. As an alternative to the laminar shock theory, Tidman[8] developed a fully turbulent shock model in which the interpenetration of cold upstream and shock heated downstream ions generated ion acoustic turbulence in the shock front. Tidman reasoned that

for high Mach numbers the laminar shock structure would break and turbulent dissipation would be required for a shock transition. However, the existence of high Mach number laminar shocks in the numerical simulations leaves open the possibility that ions reflected from a steady shock potential might be the dominant source of turbulence in electrostatic shocks.

Laboratory investigations of electrostatic shocks began with Taylor et al.[9] who studied low Mach number shocks in high T_e/T_i plasmas. They found steady laminar shock profiles that were qualitatively similar to the predictions of Moiseev and Sagdeev.[1] Means and Wong[10] and Stern and Decker[11] extended these studies to higher Mach numbers and low T_e/T_i ratios and found that a sufficient density of ions was reflected from the shock potential to generate short wavelength, high frequency ion acoustic turbulence in the shock front. Reflected ions have also been detected in experiments on high Mach number magnetosonic shocks.[12] For Alfvén Mach numbers exceeding 3.0, resistivity alone is inadequate to provide the dissipation required by the magnetosonic shock Rankine-Hugoniot relations. Several authors[13] have proposed that an electrostatic ion acoustic subshock develops on scale lengths short compared with the magnetic transition length and produces the requisite additional ion dissipation. In magnetosonic shock experiments, however, the Debye length ion acoustic subshock is not directly detectable. Hence, the properties of electrostatic shocks and reflected ion-driven wave turbulence are best investigated in magnetic field-free plasmas where Debye scale lengths are directly accessible to ordinary probe techniques.

This paper reports the results of turbulent electrostatic shock experiments performed on the University of California, Los Angeles, double plasma machine.[14] Section II discusses the experimental techniques and the laminar shock data. The experimental relationship between the Mach number and the maximum shock potential is compared with several models. The experimental values are found to lie above

those predicted by Moiseev and Sagdeev for isothermal electrons and cold ions and below those predicted by Forslund and Shonk[6] for a trapped electron distribution with cold ions. The presence of warn ions has a significant affect on the trapped electron model, but has a minimum effect on the isothermal electron model.

Section III discusses the turbulent shock structure. Three basic types of shocks were observed: 1) laminar shocks; 2) turbulent shocks in which the turbulence was small and did not significantly interact with the shock front; 3) turbulent shocks in which the turbulence became large and interacted strongly with the shock front. The three-dimensional nature of the turbulence induced by the reflected beam is also discussed along with its growth rates and spectrum.

Section IV is a theoretical discussion of the ion beam plasma stability problem. Two models are discussed: the Maxwellian beam and the truncated Maxwellian beam. Both of these models are approximations to the actual ion beam reflected by the shock potential. The group velocities of the unstable waves are also investigated. Qualitative agreement with experiment is found.

Section V is a discussion of a model of the turbulence in the shock front. We show that the Mach number vs maximum shock potential relationship cannot be explained by a theory assuming isothermal electrons even if the maximum turbulent modification of the reflected ion distribution is considered. The experimental relationship is well approximated by assuming a maximally trapped[7] electron distribution and a turbulently constructed plateau for the reflected ion distribution. Since trapped electrons are not directly detectable in the experiments, the theoretical agreement with experiment tends to confirm that trapped electrons do indeed determine the experimental shock structure.

II. EXPERIMENTAL TECHNIQUES AND MEASUREMENTS

The UCLA double plasma machine consisted of two dc discharge plasmas produced in separated cylindrical metal walled chambers. Each chamber had a diameter of 30 cm and a length of 30 cm. They were also insulated from each other and separated by a wire grid with mesh spacing less than the Debye length. The grid was biased negative so that the electrons in one plasma were isolated from electrons in the other plasma, while the ions could flow from one chamber to the other. The plasmas were in good electrical contact with the walls of the chambers which served as the anodes of the discharge current. This fixed the plasma potential in each chamber near the value of the wall potential (usually several volts above the wall potential). In practice, the walls of one chamber were grounded and a signal source was connected to the walls of the other chamber. The electron temperature in the plasma was controlled between 0.5 eV and 5.0 eV by means of a small second anode in each chamber.[14] The temperature was measured by means of a swept Langmuir probe. The ion temperature was measured by means of an electrostatic energy analyzer.[9] It was not variable and was measured to be 0.1 eV. This value was very close to the resolution of the instrument.

The plasma was a weakly ionized argon plasma with a variable density between 10^8 and $10^{10}/cm^3$. Operating conditions were usually with the density at $10^9/cm$ and a neutral pressure of 2.10^{-4} Torr. The ion charge exchange length was approximately 10 cm.

A. Shock Parameters

Since the Mach number of a shock is defined as the ratio of the velocity of the shock to the phase velocity of the small amplitude ion wave, it was necessary to produce and measure small amplitude ion acoustic waves in the

double plasma device. The ion acoustic velocity was found to be slightly less than that predicted by the linear theory $c_s = [(T_e + \gamma_i T_i)/M_i]^{1/2}$, where γ_i is an effective ion ratio of specific heats. This effect was more pronounced at low electron temperatures and is not completely understood. The discrepancy might be due to the finite size of the device and the non-Maxwellian distribution function of the electrons. The device operates with a considerable density of primary discharge electrons in the plasma. In a larger double plasma device,[15] the ion acoustic phase velocities have also been measured and the deviation from linear theory was not quite as large as in the smaller device. The Mach numbers quoted in this paper are defined as the ratios of the two experimentally measured velocities.

The shocks were generated by producing a large amplitude density step at the interface between the two plasmas. The wall potential of the rear chamber was raised by means of a voltage ramp in a time comparable to several ion plasma periods. This forced the ions in the rear chamber to flow across the interface into the front chamber where a local density excess was produced. The excess ion charge and the electrons in the front chamber interacted self-consistently to change the ion flow energy into a wave front, which then propagated away from the interface at supersonic speeds.

Figure 1 is an oscilloscope trace of a typical laminar electrostatic shock. It consists of electron density measurements as a function of time at several distances from the generating region. The reflected beam can clearly be seen in the foot structure ahead of the shock. The Mach number, density step, potential step, beam velocity, and beam density are all interrelated parameters that were experimentally measured. While the Mach number is directly measurable, the other quantities depend to some extent upon the theoretical model used to reduce the raw data.

Mach Number

The experimental relationship between the Mach number and shock potential, $e\phi/T_e$, is plotted in Fig. 2 for a large number of observed shocks. The electron temperature was varied from 0.5 eV to 5.0 eV. The Mach number dependence on electron temperature was not discernible from the experiments. The scatter due to uncertainties in determination of the Mach number and shock potential were greater than any systematic shifts detected when the electron temperature was varied.

Two theoretical curves are also shown on Fig. 2. Both are cold ion theories ($T_e/T_i = \infty$). Moiseev and Sagdeev[1] assumed isothermal electrons and arrived at the result

$$M^2 = \frac{1}{2} \frac{[\exp(e\phi/T_e) - 1.0]^2}{\exp(e\phi/T_e) - 1.0 - e\phi/T_e} \quad . \tag{1}$$

Forslund and Shonk[6] assumed a trapped electron distribution function with the equation of state

$$P(e\phi/T_e)/P_0 = 2(e\phi/T_e)^{1/2}/\sqrt{\pi} + \exp(e\phi/T_e)\mathrm{erfc}[(e\phi/T_e)^{1/2}] + 4(e\phi/T_e)^{3/2}/3\sqrt{\pi} \tag{2}$$

and arrived at the Mach number given by

$$M^2 = \frac{1}{2} \frac{(P - 1.0)^2}{(P - 1.0 - e\phi/T_e)} \quad . \tag{3}$$

The experimental data lie between these two theoretical curves.

The effect of the finite electron to ion temperature ratio was investigated by Bardotti and Segre[1,2] for the case of isothermal electrons and Maxwellian ions. In order to compare their calculations with this experiment, the Mach number in their published data must be divided by the ion temperature correction factor for linear ion acoustic waves. This factor was computed

by Bardotti and Segre[1] to be $(1.0 + 3.4\ T_i/T_e)$. When this was done, the resulting relationship between Mach number and shock potential differed only slightly from that predicted by Moiseev and Sagdeev for cold ions, and hence disagrees with experiment.

The finite ion temperature corrections to the Mach number -- potential relationship for the trapped electron distribution were calculated assuming that the reflected ion distribution was a truncated Maxwellian. For $T_e/T_i \gtrsim$ 15 to 50, the theoretical curves agree roughly with the experimental data (Fig. 3). However, no direct observation of trapped electrons has been possible in the experiments. Hence, the question remains of whether turbulent relaxation of the reflected ion distribution could sufficiently modify the isothermal electron shock theory to bring its predictions into agreement with experiment. In Sec. V.0 we develop a model for the turbulent dissipation of the reflected ions and demonstrate that only the trapped electron distribution yields agreement with experiment.

Reflected Ion Density and Velocity

The number of ions reflected from the shock can be computed from energy considerations. In the wave frame, the shock front is a potential barrier of height $e\phi$, so that all particles with velocity less than $(2e\phi/M_i)^{1/2}$ will be reflected. Let us assume that the incoming ions are Maxwellian with a temperature T_i; then, the number density of reflected particles is

$$\frac{n_b}{n_0} = \frac{1}{\sqrt{\pi}\ a_i} \int_{v_1}^{v_2} dv\ \exp(-v^2/a_i^2) \tag{4}$$

where $a_i = (2T_i/M_i)^{1/2}$ is the ion thermal speed, $v_1 = [MC_s - (2e\phi/M_i)^{1/2}]$, $v_2 = MC_s$, and n_0 is the upstream plasma density. The average velocity of the reflected particles is also calculated straightforwardly to get

$$v_b \equiv \langle v \rangle = \frac{\int_{v_1}^{v_2} dv\, v\exp(-v^2/a_i^2)}{\int_{v_1}^{v_2} dv\, \exp(-v^2/a_i^2)} \quad . \tag{5}$$

These relationships, (4) and (5), are indeterminate for a given shock wave unless the relationship between Mach number and shock potential height $e\phi/T_e$ is known. For the experimental relationship $M = 1.0 + 0.6\ e\phi/T_e$, the density of reflected ions was calculated and plotted in Fig. 4 for the temperature ratios $T_e/T_i = 10$ and 30. The predicted beam densities from Sagdeev's cold ion relationship between Mach number and shock potential are also shown. Figure 5 shows the calculated beam velocities versus the shock potential jump for these temperature ratios. The beam velocity was measured by two independent methods. The velocity of the foot structure in front of the shock wave was measured directly on the oscilloscope traces of the data such as that in Fig. 1. It was also measured with an energy analyzer by sampling techniques. These measurements were generally within 15% of one another.

The measured beam densities agree with those values predicted by the experimental relationships between Mach number and shock potential height. This demonstrates the self-consistency of the measurements, and that the beam ions ahead of the shock come as a result of reflection and not from other sources (e.g., streaming ions from the generating region). There were only small differences in the beam velocities predicted by the different theoretical models. The experimental uncertainty in beam velocity was larger than such differences.

III. TURBULENT SHOCK STRUCTURE

Three qualitatively different shocks were observed in the course of the experiments: 1) laminar shocks in which no turbulence existed; 2) turbulent shocks in which the turbulence remained small (much less than the shock height) and did not significantly interact with the shock front; 3) turbulent shocks in which the turbulence grew to a level comparable to the shock height. There was considerable interaction between the turbulence and the shock front in the third type.

Earlier, Fig. 1 was referred to as a typical laminar shock. It has few reflected ions, a small Mach number, a periodic trailing wave train, and no turbulence. It is the electrostatic shock discussed in most computer simulation studies and in most theories.

Figure 6 is an oscilloscope trace of a turbulent shock in which the turbulence remained small and did not significantly interact with the shock front. The turbulence was primarily confined to the reflected beam region which extended ahead of the shock front. The oscilloscope trace is a superposition of many shocks and the turbulence is shown as the blurred region in the photograph. (The system was run at a repetition rate of 1 kHz.) Each trace is a time profile of the shock at a different distance from the interface between the two plasmas. At $x = 2$ cm, the shock appeared laminar; the reflected beam was evident and there existed a trailing wave train. Down the chamber at $x = 4$ cm, the first evidence of turbulence appeared in the foot structure ahead of the shock front. Farther down the chamber the turbulence became more pronounced and the trailing wave train disappeared. The turbulence always remained much less than the main shock front height.

Figure 7 is a set of oscilloscope traces of the third type of shock. The turbulence grew to a level comparable to the shock front and interacted strongly

with it. Since the display is a superposition of many shocks, the turbulence again appears as the blurred region in the photograph. Individual shocks were studied on a storage oscilloscope and the turbulence became more apparent. These oscilloscope traces are shown in Figs. 8 and 9. Again the shock is laminar close to the interface region.[16] The reflected beam was present and there was no trailing wave train. As the shock traveled down the chamber, the turbulence grew to a level comparable to the shock potential. It was no longer confined to the reflected beam region and the shock had a broad turbulent transition region between the upstream and downstream states.

Figure 10 is a plot of the normalized amplitude of the shock front as a function of distance for the three types of observed shocks. There was a decay of the shock as it propagated down the chamber due to geometrical effects and charge exchange. The laminar shock and the small amplitude turbulence shock appeared similar in this respect. On the other hand, the large amplitude turbulence shock decayed more rapidly. As the shock propagates into the target plasma, it sweeps-up target plasma ions which then eventually form the reflected ion beam. This time-dependent energy exchange between the shock and reflected ions is analogous to linear Landau damping. Since the large amplitude turbulence shocks generally have larger shock potentials and occur for lower T_e/T_i, they reflect a larger fraction of the upstream ions than do the laminar and small turbulent amplitude shocks; hence, the large amplitude turbulent shocks should undergo a larger spatial damping. Another aspect of the turbulent shocks is that the turbulence appeared to be almost stationary with respect to the shock front. This will be discussed further in Sec. IV where the ion beam plasma dispersion relation is considered.

The growth rates of the turbulence and the spectra have been measured and reported earlier.[10] It was possible to make detailed measurements of growth

rates at a particular frequency and wavelength, with the direction of propagation known, by propagating a small ion acoustic wave packet ahead of the shock. Qualitative agreement was found with the ion beam-plasma theory developed in Sec. IV. Quantitative agreement with the theory was found only within a factor of two. The limitations of this theory are discussed in Sec. IV.

The observations of turbulence in these experiments depended fundamentally upon the three-dimensional nature of the plasma. The reflected ion beam was able to interact with ambient noise ion waves which were traveling at angles to the beam velocity. This allowed a resonant interaction between the beam and the waves which resulted in the growth of the turbulence. The average propagation direction of the turbulent spectra in front of the shock wave was difficult to measure since parameters determining that direction, such as beam velocity, could not be controlled over a wide range of values. To surmount these difficulties, the double plasma machine was used to create a steady state ion beam with a given velocity traversing the front chamber by biasing the wall of the rear chamber positive. This approximated the region in front of the shock wave. Under such conditions there was ion acoustic turbulence in the front chamber.[17] The direction of wave propagation was measured by a disk shaped Langmuir probe with a diameter large compared to the wavelength of the dominant turbulent modes. A wave which propagated parallel to the face of the probe was averaged out over the surface. A wave which propagated perpendicular to the probe face was detected. Rotating the probe until the maximum signal was obtained gave the most probable direction of wave propagation. This angle is plotted in Fig. 11. Two theoretical curves are also shown in Fig. 11. These will be discussed further in Sec. IV. The most important point of the data shown is that the largest amplitude waves propagated at large angles to the beam. This emphasized the critical nature of the three dimensionality to the observation of the turbulent shocks.

In the one-dimensional computer simulations of electrostatic shocks by Sakanaka, et al.,[18] Mason,[19] and Forslund and Shonk,[6] the turbulence due to reflected beam has been seen only once.[20] We believe that this was primarily due to the one-dimensional character of their plasmas. Furthermore, in those cases where there was a possibility that turbulence could develop in a one-dimensional situation (i.e., at low temperature ratios), only a small number of computer simulations were run, and the shocks were followed for only a small distance. (Much of the simulation has been done at high temperature ratios. Only a few ions were reflected in these cases.) From the profiles of the turbulent shocks in Figs. 6 and 7, it is clear that the shock wave had to propagate a considerable distance into the plasma before the turbulence developed. This was simply due to the fact that the beam had to exist for a finite length ahead of the shock in order for the wave to grow over many wavelengths. The computer simulations usually stopped long before this could happen.

IV. ION BEAM-PLASMA STABILITY ANALYSIS

In general, the plasma ahead of the shock is unstable to ion acoustic waves for an ion beam within only a limited range of parameters. For small beam densities and $T_e > T_i$, the interaction between the wave and the beam is primarily a resonant interaction. For instability to occur it is necessary for the slope of the distribution function to be positive. In a one-dimensional plasma with Maxwellian distribution functions for the plasma and the beam this requirement is

$$\frac{r(V_b-C_s)}{C_s} \exp\left[\frac{-(V_b-C_s)^2}{a_i^2} + \frac{T_e}{2T_i}\right] > 1.0 \qquad (6)$$

where V_b is the veam velocity, C_s is the ion acoustic velocity, r is the ratio of beam density to ion density, and $a_i = [2T_i/M_i]^{1/2}$ is the ion thermal velocity. Equation (6) states that V_b must be greater than C_s for an instability to occur. The beam velocity, however, cannot be too large, since then the term in the exponential becomes negative and dominates. An upper limit to the beam velocity is near 2.0 C_s. Thus, for a one-dimensional plasma the beam velocity must be approximately between the ion acoustic speed and twice the ion acoustic speed.

The limitation that the beam velocity must be approximately between the ion acoustic speed and twice the ion acoustic speed is true only in a one-dimensional plasma. For a three-dimensional plasma in which waves can travel at an angle θ to the beam, this condition is relaxed to that of $C_s \lesssim V_b \cos\theta \lesssim 2C_s$, or

$$\cos^{-1}(C_s/V_b) \lesssim \theta \lesssim \cos(2C_s/V_b) \quad . \qquad (7)$$

The unstable ion wave growth rates and the onset of turbulence were computed by the three-dimensional dispersion relation considered by Fried and Wong[21]

for a homogeneous beam plasma system

$$\varepsilon(k,\omega) \equiv 1 - \sum_{\alpha} \frac{\omega_\alpha^2}{k^2} \int \frac{dv\ \underline{k} \cdot \frac{\partial f_{i\alpha}}{\partial \underline{v}}}{\underline{k} \cdot \underline{v} - \omega} = 0 \tag{8}$$

where species α has distribution function f_α and plasma frequency ω_α. If Maxwellian distribution functions are assumed and we specialize to the case where the ions of the plasma and the beam have equal mass and temperature, Eq. (8) becomes

$$\frac{2k^2}{k_{D_i}^2} = Z' \left(\frac{\omega}{ka_i} \right) + r\ Z' \left(\frac{\omega - \underline{k} \cdot \underline{V}_b}{ka_i} \right) - 2(1+r) \frac{T_i}{T_e} \tag{9}$$

where $\underline{V}_b$ is the beam velocity, k_{D_i} is the ion Debye wave number $(4\pi n_i e^2/T_i)^{1/2}$, and $Z'(s)$ is the derivative of the plasma dispersion function. It has also been assumed that the phase velocity ω/k is small compared with the electron thermal velocity. The Maxwellian assumption for the beam ions is only an approximation to the actual case.

The ion waves tend to propagate in the direction which will maximize their growth rate. This allows us to solve the dispersion relation for $\underline{k}$ parallel to the beam direction as if in a one-dimensional theory. The maximum growth rates obtained can be projected back onto the angle at which the wave propagates. For example, if for a given beam density and temperature ratio it was found that one-dimensional growth rate was maximum near the beam velocity $V_b = 1.1\ C_s$, and if the actual beam in the plasma was traveling at $2.0\ C_s$, then the direction of propagation of the maximally unstable wave would be given by $\theta = \cos^{-1}(1.1/2.0) = 57°$. Figure 12 is a plot of maximum growth rate (maximized as a function of frequency) vs beam density at $V_b/C_s = 1.0$. Since the growth rate was generally a maximum near $V_b/C_s = 1.0$ these data can be also considered as a density stability limit graph.

The group velocity of the turbulent waves was experimentally found to be near the shock wave velocity, especially for the type 2 turbulent shocks. In the presence of unstable modes the group velocity is not a theoretically well defined quantity. In the limit of small growth rates, however, an expression can be arrived at from a variational principle which yields

$$V_{g_x} = \frac{\delta\omega}{\delta k_x} = - \frac{\partial \varepsilon_r}{\partial \underline{k}_r} \cdot \hat{x} \Big/ \frac{\partial \varepsilon_r}{\partial \omega} \quad . \tag{10}$$

From Eq. (8) this gives the group velocity in the beam direction

$$\frac{\delta\omega}{\delta k} = \frac{\omega}{k_r} \cos\theta + \frac{\dfrac{2k_r^2 a_i^3}{\omega_{p_i}^2} \cos\theta + rV_b \sin^2\theta \, Z'' \left(\dfrac{\omega - \underline{k}_r \cdot \underline{V}_b}{k_r a_i} \right)}{Z'' \left(\dfrac{\omega}{k_r a_i} \right) + rZ'' \left(\dfrac{\omega - \underline{k}_r \cdot \underline{V}_b}{k_r \cdot a_i} \right)} \quad . \tag{11}$$

Two group velocity versus frequency curves are plotted in Fig. 13 for typical experimental situations. Linear theory with no ion beam present predicts group velocities on the order of 0.5 C_s. Figure 13 shows that the presence of a small beam increases the group velocity. Hence, the observed tendency of the ion acoustic turbulence to propagate with group speeds comparable to the shock speed is qualitatively consistent with ion beam instability theory. However, it has not been possible to differentiate between type 2 and 3 turbulent shocks on the basis of the present linear stability analysis. First, the experimental reflected ion distribution is not Maxwellian, whereas the group speed calculations are very sensitive to the shape of the reflected ion distribution function through the $Z'' \left(\dfrac{\omega - \underline{k}_r \cdot \underline{V}_b}{k a_i} \right)$ term. Second, the reflected beam-plasma interaction is not completely steady with the beam, shock, and turbulence all interacting as the shock propagates down the chamber. Finally, additional detailed measurements of the angular distribution of the turbulent waves and the spatial

structure of the reflected ion distribution function are needed to more clearly differentiate between the two types of turbulent shocks.

A. Stability Analysis of a Truncated Maxwellian

In the shock frame, if the upstream ions have a Maxwellian distribution, ions with kinetic energy per unit charge less than the maximum shock potential will be reflected back upstream. If these ions are specularly reflected from a steady shock front, the upstream ion distribution in the direction normal to the shock front (x direction) would be a truncated Maxwellian between the edge velocity $-v_0(x) = -[2e/M_i(\bar{\phi}(0) - \bar{\phi}(x))]^{1/2} \leq v_x \leq \infty$ given by

$$f_i = \frac{1}{\pi^{3/2} a_i^3} \exp(-v_\perp^2/a_i^2) \begin{cases} \exp\left(-\frac{1}{a_i^2}\left[\left(v_x^2 + \frac{2e\phi(x)}{M_i}\right)^{1/2} - u_0\right]^2\right) & -v_0(x) \leq v_x \leq \infty \\ 0 & -v_x \leq -v_0(x) \end{cases} \tag{12}$$

$\bar{\phi}(x)$ is the local shock potential, $\bar{\phi}(0)$ is the maximum shock potential assumed to occur at $x = 0$, u_0 is the upstream flow speed, directed toward positive x, $v_\perp$ is the velocity magnitude perpendicular to the shock normal, a_i is the ion thermal speed and f_i is normalized to unity. In order to investigate the stability of f_i to ion acoustic perturbations, we assume that the waves and linearized electron and ion distribution functions can be expanded in WKB eigenfunctions (see Sec. V) and thereby obtain the local electrostatic dielectric function

$$\varepsilon(\omega,\underline{k}) = 1 + \frac{\exp(e\bar{\phi}/T_e)}{k^2\lambda_D^2} + \frac{\omega_{p_i}^2}{k^2} \int \frac{\underline{k} \cdot \frac{\partial f_i}{\partial \underline{v}}\, d^3v}{\omega - \underline{k} \cdot \underline{v}} \tag{13}$$

where $\lambda_D = c_s/\omega_{p_i}$, $c_s^2 = T_e/M_i$, $\omega_{p_i}^2 = \frac{4\pi n_e e^2}{M_i}$ with n_e being the upstream electron

density. Introducing the above ion distribution function, performing the integrals over $d^2v_\perp$, and integrating by parts with respect to dv_x, the dispersion relation can be written as

$$0 = k^2 + \exp\left(\frac{e\bar{\phi}(x)}{T_e}\right) - \frac{T_e}{T_i}\frac{k^2}{k_\perp k_x}\int_{-t_1}^{\infty} dt\,\frac{\partial G}{\partial t}\,Z\left(\frac{\omega - k_x M_* t}{k_\perp (2T_i/T_e)^{1/2}}\right) -$$

$$- \frac{T_e}{2T_i}\,\frac{k_\perp}{k_x}\,G(-t_1)\,Z\left(\frac{\omega + k_x M_* t_1}{k_\perp\,(2T_i/T_e)^{1/2}}\right) \qquad (14)$$

where the wave numbers k_x, $k_\perp$, and k have been normalized to λ_D, the frequency ω has been normalized to ω_{p_i}, and $M_* = u_0/c_s$ is the sonic Mach number. The function G(t) is given by

$$G(t) = \begin{cases} \frac{1}{\sqrt{\pi}} \exp\left[- \frac{u_0^2}{a_i^2}\left[\left(t^2 + \frac{2e\bar{\phi}(x)}{M_I^2 T_e}\right)^{1/2} - 1\right]^2 \right] & -t_1 \le t \le \infty \\ 0 & t < -t_1 \end{cases} \qquad (15)$$

where $t_1 = 1/M_* \left[2e\left(\bar{\phi}(0) - \bar{\phi}(x)\right)\right]^{1/2}$.

The dispersion relation was solved as a function of shock potential $\bar{\phi}(x)$ for real ω (in the shock frame) and $k_\perp$, complex k_x, $T_e/T_i = 20$, and $M_* = 1.46$. Figure 14 shows the spatial growth rate Im k_x vs $\bar{\phi}(x)$ for Re $k_x = 1$, and variable $k_\perp$. The growth rates are largest near the maximum shock potential, as expected, since the relative velocity between the incident and reflected ions is smallest there. Furthermore, the oblique waves $k_\perp > k_x$ are most unstable, as in the homogeneous calculations of Sec. IV-A. The very large growth rates indicate that the reflected ions will rapidly lose their momentum to the unstable ion waves and their distribution function will spatially evolve to a marginally stable form. Hence, upstream from the shock the reflected ion distribution should approach a quasi-plateau.

V. ION BEAM TURBULENCE AND SHOCK STRUCTURE

In Sec. III we showed that the experimental mach number vs shock potential relationship was in rough agreement with a steady state shock theory involving a Maxwellian distribution for incident and reflected ions and the maximal trapping electron equation of state. This theory, however, did not include the effects of the unstable ion beam turbulence and the turbulent modification of the reflected ion distribution function. Since measurements of the electron distribution function were not capable of detecting the presence of trapped electrons, the question remains as to whether turbulent ion dynamics could explain the Mach number-potential relationship even with isothermal electrons. An additional question is to what extent the shock structure calculated with trapped electrons is modified by ion acoustic turbulence.

In order to resolve these questions, in this section we derive a differential equation for the steady state shock structure which includes the ion beam turbulence. We assume that the unstable ion waves are propagating with a finite group velocity in the shock frame. Hence, the calculations apply to the second type of turbulent shock of Sec. III, but probably do not apply to the first type of turbulent shock in which the waves appear to have an almost zero group speed in the shock frame. We treat the wave dynamics in the quasi-linear approximation using WKB spatial eigenfunctions. Rather than solve for the turbulent modification of the reflected ion distribution function, we assume that the wave turbulence has flattened the distribution function across the resonant velocity region and use flux conservation to determine the velocity width of the plateau. This assumption yields an upper limit to the turbulent modification of the shock structure.

Quasilinear Equations

We assume that in the co-moving frame the shock has a steady, time-averaged spatial structure which depends only on the direction x normal to the shock front; $x = -\infty$ is upstream and $x = 0$ is the first maximum in the steady electrostatic potential. We can then write the Vlasov-Poisson equations for the steady (fluctuating) particle distribution functions $\bar{f}(\underline{v},x)$ $[f_1(\underline{v},\underline{r})]$ and potential $\bar{\phi}(x)[\phi_1(\underline{r},\underline{t})]$ as

$$v_x \frac{\partial \bar{f}_\alpha}{\partial x} - \frac{q_\alpha}{m_\alpha} \frac{\partial \bar{\phi}}{\partial x} \frac{\partial \bar{f}_\alpha}{\partial v_x} = \frac{q_\alpha}{m_\alpha} \overline{(\nabla \phi_1) \frac{\partial f_{1\alpha}}{\partial \underline{v}}} \tag{16}$$

$$\frac{d^2 \bar{\phi}}{dx^2} = -4\pi \sum_\alpha q_\alpha \int \bar{f}_\alpha \, d^3v \tag{17}$$

$$\frac{\partial f_{1\alpha}}{\partial t} + \underline{v} \cdot \nabla f_{1\alpha} - \frac{q_\alpha}{m_\alpha} \frac{\partial \bar{\phi}}{\partial x} \frac{\partial f_{1\alpha}}{\partial v_x} = \frac{q_\alpha}{m_\alpha} (\nabla \phi_1) \frac{\partial \bar{f}_\alpha}{\partial \underline{v}} \tag{18}$$

$$-\nabla^2 \phi_1 = 4\pi \sum_\alpha q_\alpha \int f_{1\alpha} \, d^3v \tag{19}$$

where $q_\alpha = \pm e$ is the electronic charge for ions (+) and electrons (-), m_α is the specific mass, and $\sum_\alpha$ is the sum over ions and electrons. Equation (18) is the linearized Vlasov equation.

Linear Solution

For low Mach number shocks, the scale length of the shock front is somewhat larger than the wavelength of the unstable turbulence, which is comparable to the Debye length λ_D. Therefore to obtain an approximate equation for the shock structure we choose WKB solutions to the linear equation in the form

$$f_{1,\alpha}(\underline{v},\underline{r},t) = \sum_\omega f_{\omega,\alpha}(x,\underline{v}) \exp\left[i \int_{-\infty}^{x} k_x(x')dx' + ik_y y - i\omega t \right] \tag{20}$$

$$\phi_1(\underline{r},t) = \sum_{\omega} \phi_\omega(x) \exp\left[i \int_{-\infty}^{x} k_x(x')dx' + ik_y y - i\omega t \right] \tag{21}$$

where $f_{\omega,\alpha}$, $\phi_\omega(x)$ are slowly varying WKB amplitudes, $k_x(x)$ is the complex, spatially dependent wave number in the x direction, k_y is the y-direction wave number, and ω is the real eigenfrequency. For simplicity, we only consider two-dimensional wave propagation.

By the WKB assumption, $\partial/\partial x(f_{\omega,\alpha}, \phi_\omega)$ is small compared with $k_x(f_{\omega,\alpha}, \phi_\omega)$. Therefore, we solve Eq. (18) by iteration by writing $f_{\omega,\alpha} = f^{(1)}_{\omega,\alpha} + f^{(2)}_{\omega,\alpha}$ where $f^{(1)}_{\omega,\alpha}$ is order k_x and $f^{(2)}_{\omega,\alpha}$ is order $\partial/\partial x$. After substitution into (18), we find

$$f^{(1)}_{\omega,\alpha} = -q \frac{k_x v_x \frac{\partial \bar{f}_\alpha}{\partial W_x} + k_y v_y \frac{\partial \bar{f}_\alpha}{\partial W_y}}{\omega - k_x v_x - k_y v_y} \tag{22}$$

$$f^{(2)}_{\omega,\alpha} = \frac{iq_\alpha v_x \left[(\omega - k_y v_y) \frac{\partial \bar{f}_\alpha}{\partial W_x} + k_y v_y \frac{\partial \bar{f}_\alpha}{\partial W_y} \right]}{\omega - k_x v_x - k_y v_y} \frac{\partial}{\partial x} \left(\frac{\phi_\omega}{\omega - k_x v_x - k_y v_y} \right) \tag{23}$$

where $W_x = \frac{m_\alpha v_x^2}{2} + q_\alpha \bar{\phi}(x)$, $W_y = \frac{m_\alpha v_y^2}{2}$. In Eq. (23), the x dependence of $\bar{f}_\alpha(W_x, W_y, x)$ has been neglected since it arises solely from the wave turbulence, and hence is second order in ϕ_ω. After substitution of (21), (22), and (23), Eq. (19) can be solved to first order in $\partial/\partial x$ to obtain

$$k^2 \varepsilon(\underline{k},\omega) |\phi_\omega|^2 - i \frac{d}{dx} \left(\frac{k^2}{2} \frac{\partial \varepsilon(\underline{k},\omega)}{\partial k_x} |\phi_\omega|^2 \right) = 0$$

$$\varepsilon(\underline{k},\omega) = 1 + \frac{1}{k^2} \sum_\alpha 4\pi q_\alpha^2 \int d^2v \frac{k_x v_x \frac{\partial \bar{f}_\alpha}{\partial W_x} + k_y v_y \frac{\partial \bar{f}_\alpha}{\partial W_y}}{\omega - k_x v_x - k_y v_y} \tag{24}$$

$$\equiv 1 + \frac{1}{k^2} \sum_\alpha D_\alpha$$

The lowest order in $\partial/\partial x$ solution $\varepsilon(\underline{k},\omega) = 0$ determines the complex wave number $k = (k_x^2 + k_y^2)^{1/2}$; the next order in $\partial/\partial x$ specifies that $\left(\frac{k^2}{2}\frac{\partial\varepsilon}{\partial k_x}|\phi_\omega|^2\right)$ is constant, and thus determines the spatial dependence of the WKB amplitude $|\phi_\omega|^2$. If the imaginary parts of k and ε are small, then we only need $\mathrm{Re}\left(\frac{k^2}{2}\frac{\partial\varepsilon}{\partial k_x}|\phi_\omega|^2\right) = \text{const.}$

Equation for the Shock Structure

We now derive an equation for the shock potential $\bar{\phi}$, which includes the unstable wave turbulence driven by the reflected ions. We first multiply Eq. (16) $m_\alpha v_x$, integrate over velocity space, and then sum over species to find

$$\frac{d}{dx}\left(\sum_\alpha m_\alpha \int d^2v\, v_x^2\, \bar{f}_\alpha\right) + \sum_\alpha q_\alpha \frac{d\bar{\phi}}{dx}\int d^2v\, \bar{f}_\alpha + \hat{e}_x \sum_\alpha q_\alpha \overline{(\nabla\phi_1)\int d^2v\, f_{1\alpha}} = 0 \qquad (25)$$

where $\hat{e}_x$ is a unit vector in the x direction. We now eliminate $\sum_\alpha q_\alpha \int d^2v\, \bar{f}_\alpha$ $\left[\sum_\alpha q_\alpha \int f_{1\alpha}\, d^2v\right]$ by Eqs. (17) [(19)], substitute (21) for $\phi_1(\underline{r},t)$, and perform the time average in the last term. If we then write $k_x(x)$ as $k_x = k_x^r + ik_i$, expand the last term in (25) in order d/dx taking k_i of order d/dx, and take the real part of the result, (25) becomes

$$\frac{dP_e}{dx} + \frac{d}{dx}\left(M_i \int d^2v\, v_x^2\, \bar{f}_i\right) - \frac{1}{8\pi}\frac{d}{dx}\left(\frac{d\bar{\phi}}{dx}\right)^2 + \sum_\omega \left\{ k^2 \frac{d}{dx}\left(\frac{|\phi_\omega|^2}{8\pi} \exp\left(-2\int_{-\infty}^{x} k_i\, dx'\right)\right) - \right.$$

$$\left. - \frac{k_x}{4\pi}\exp\left(-2\int_{-\infty}^{x} k_i\, dx'\right)\frac{d}{dx}\left(k_x|\phi_\omega|^2\right)\right\} = 0 \quad . \qquad (26)$$

In (26) we have neglected the electron inertia term and retained only the electron pressure P_e; for simplicity, we have changed notation to write $k_x \equiv k_x^r$, $k^2 = (k_x^r)^2 + k_y^2$. Equation (26) can be integrated with the boundary

condition that $d/dx = 0$ at $x = -\infty$

$$(P_e + M_i \int d^2v\, v_x^2\, \bar{f}_i)_{-\infty}^{x} - \frac{1}{8\pi}\left(\frac{d\bar{\phi}}{dx}\right)^2 + \int_{-\infty}^{x} dx' \sum_{\omega} \left\{ k^2 \frac{d}{dx'}\left[\frac{|\phi_\omega|^2}{8\pi} \exp(-2\int_{-\infty}^{x'} k_i\, dx'') \right] - \right.$$

$$\left. - \frac{k_x}{4\pi} \exp(-2\int_{-\infty}^{x'} k_i\, dx'')\ \frac{d}{dx'}(k_x |\phi_\omega|) \right\} = 0 \quad . \tag{27}$$

To determine P_e, we form the momentum moment of the electron equation (16), substitute (22) and (23) for $f_{1,e}$ and perform the time average and the integrals over velocity to find

$$\frac{dP_e}{dx} - e\bar{n}_e \frac{d\bar{\phi}}{dx} = -\frac{1}{4\pi} \sum_{\omega} \left(i(k_x - ik_i)\phi_\omega^* - \frac{d\phi_\omega^*}{dx} \right)[D_e\phi_\omega - i \frac{\partial D_e}{\partial k_x} \frac{d\phi_\omega}{dx} -$$

$$- \frac{i}{2} \frac{d}{dx}\left(\frac{\partial D_e}{\partial k_x}\right) \phi_\omega] \exp(-2\int_{-\infty}^{x} k_i\, dx) \tag{28}$$

where $\bar{n}_e = \int d^2v\, \bar{f}_e$. Since the unstable waves have phase speeds on the order of the ion acoustic speed $c_s = [T_e/M_i]^{1/2}$ and are driven by ion streaming, Im D_e << Re D_e; hence, neglecting Im D_e and taking the real part (28) yields

$$\frac{dP_e}{dx} - e\bar{n}_e \frac{d\bar{\phi}}{dx} = \sum_{\omega} \left\{ \text{Re } D_e \frac{d}{dx}\left(\frac{|\phi_\omega|^2}{8\pi} \exp(-2\int_{-\infty}^{x} k_i\, dx) \right) - \right.$$

$$\left. - \frac{k_x}{8\pi} \frac{d}{dx}\left(\frac{\partial D_e}{\partial k_x} |\phi_\omega|^2 \right) \exp(-2\int_{-\infty}^{x} k_i\, dx) \right\} \quad . \tag{29}$$

If we assume that the electrons are approximately isothermal $P_e = n_e(x)T_e$ with T_e = const, (29) can be integrated with respect to x from $-\infty$ to x

$$P_e(x)\Big|_{-\infty}^{x} = \bar{n}_e(-\infty)T_e \left\{ \exp(e\bar{\phi}/T_e)\, \exp\left\{ \int_{-\infty}^{x} dx' \sum_{\omega} \frac{\mathrm{Re}D_e}{\bar{n}_e T_e} \frac{d}{dx'} \left[\frac{|\phi_\omega|^2}{8\pi} \exp(-2\int_{-\infty}^{x'} k_i dx'' \right] \right.\right.$$

$$\left.\left. - \frac{k_x}{8\pi \bar{n}_e T_e} \frac{d}{dx'} \left[\frac{\partial \mathrm{Re}\, D_e}{\partial k_x} |\phi_\omega|^2 \right] \exp(-2\int_{-\infty}^{x'} k_i\, dx'') \right\} - 1 \right\} \qquad (30)$$

For weak turbulence and low Mach number shocks, $e^2|\phi_\omega|^2/T_e^2 \ll 1$. Furthermore, the x' dependence of the integrand in (30) will be dominated by the exponential $\exp(-2\int_{-\infty}^{x'} k_i dx'')$. Hence, we can take $\bar{n}_e(x') \tilde{\approx} \bar{n}(x)$ outside the integrand, and expand the exponential to lowest order in $|\phi_\omega|^2$ to find

$$P_e(x)\Big|_{-\infty}^{x} = \bar{n}_e(-\infty)T_e \left(\exp(e\bar{\phi}/T_e) - 1 \right) + \int_{-\infty}^{x} dx' \sum_{\omega} \left\{ \mathrm{Re}\, D_e \frac{d}{dx'} \left[\frac{|\phi_\omega|^2}{8\pi} \exp(-2\int_{-\infty}^{x'} k_i dx'') \right] \right.$$

$$\left. - \frac{k_x}{8\pi} \frac{d}{dx'} \left[\frac{\partial \mathrm{Re}\, D_e}{\partial k_x} |\phi_\omega|^2 \right] \exp(-2\int_{-\infty}^{x'} k_i dx'') \right\} \qquad (31)$$

To determine the ion contribution $M_i \int d^2v\, v_x^2\, \bar{f}_i\Big|_{-\infty}^{x}$ in Eq. (27) we form the momentum moment of (16), substitute (22) and (23), time average and take the real part of the result to find

$$\frac{d}{dx}\left[M_i \int d^2v\, v_x^2\, \bar{f}_i \right] + e\bar{n}_i \frac{d\bar{\phi}}{dx} = \frac{1}{4\pi} \sum_{\omega} \left\{ \mathrm{Re}\, D_i \left[k_i |\phi_\omega|^2 - \frac{1}{2} \frac{d|\phi_\omega|^2}{dx} \right] - \right.$$

$$\left. - k_x\, \mathrm{Im}\, D_i\, |\phi_\omega|^2 + \frac{k_x}{2} \frac{\partial \mathrm{Re}D_i}{\partial k_x} \frac{d|\phi_\omega|^2}{dx} + \frac{k_x}{2} \frac{d}{dx} \left(\frac{\partial \mathrm{Re}D_i}{\partial k_x} \right) |\phi_\omega|^2 \right\} \exp(-2\int_{-\infty}^{x} k_i dx') \qquad (32)$$

Substituting the quaslinear relation $k_i = -\mathrm{Im}\, D_i/(\partial \mathrm{Re}\varepsilon/\partial k_x)$ and integrating (17) over x we find

$$M_i \int d^2v\, v_x^2\, \bar{f}_i \Big|_{-\infty}^{x} = -e \int_0^{\bar{\phi}(x)} \bar{n}_i(\phi')d\phi' + \int_{-\infty}^{x} dx' \sum_\omega \Bigg\{ \mathrm{Re}\, D_i \frac{d}{dx'} \Bigg[\frac{|\phi_\omega|^2}{8\pi} \exp(-2\int_{-\infty}^{x'} k_i dx'') -$$

$$+ k_x \frac{d}{dx'} \Bigg[\frac{k^2 \frac{\partial \mathrm{Re}\varepsilon}{\partial k_x} |\phi_\omega|^2}{8\pi} \exp(-2\int_{-\infty}^{x'} k_i dx'' \Bigg] - \frac{k_x}{8\pi} \exp(-2\int_{-\infty}^{x'} k_i dx'') \frac{d}{dx'} \left(\frac{\partial \mathrm{Re} D_i}{\partial k_x} \right) \Bigg\} \tag{33}$$

where $\bar{n}_i$ has been written as a function of the potential $\bar{\phi}$.

We can now combine (27), (31), and (33) to obtain the desired equation for $\bar{\phi}$. If we normalize the variables as $\psi = e\bar{\phi}/T_e$, $x \to x/\lambda_D$, $k \to k\lambda_D$, and $\psi_\omega = e\phi_\omega/T_e$, we obtain

$$\frac{1}{2}\left(\frac{d\psi}{dx}\right)^2 = e^\psi - 1 - \int_0^\psi d\psi' \frac{\bar{n}_i(\psi')}{\bar{n}_e(-\infty)} + \int_{-\infty}^{x} dx' \sum_\omega k_x \frac{d}{dx'} \left[\frac{k^2 \frac{\partial \mathrm{Re}\varepsilon}{\partial k_x} |\phi_\omega|^2}{2} \exp(-2\int_{-\infty}^{x'} k_i dx'') \right] . \tag{34}$$

The local dispersion relation $\varepsilon(k,\omega) = 0$ was used in reducing the turbulence terms. Equation (34) is an implicit equation for ψ and would be self-consistent if the ψ dependence of $\varepsilon(\underline{k},\omega)$ and k_i were known. If we assume that $k_x(x)$ is only weakly dependent on x, we can replace k_x by an average value k_x^* and perform the x integration to obtain

$$\frac{1}{2}\left(\frac{d\phi}{dx}\right)^2 \equiv -V(\psi) \equiv e^\psi - 1 - \int_0^\psi d\psi' \frac{\bar{n}_i(\psi')}{\bar{n}_e(-\infty)} + \sum_\omega \frac{k_x^* k^2}{2} \frac{\partial \mathrm{Re}\varepsilon}{\partial k_x} |\phi_\omega|^2 \left[\exp(-2\int_{-\infty}^{x} k_i dx') - 1 \right] \tag{35}$$

where $V(\psi)$ is the nonlinear quasipotential. $V(\psi) = 0$ occurs at the upstream point $\psi = 0$ and at the first maximum of the potential $\psi(0)$. The condition for a steady shock solution to (35) is that $V(\psi)$ be negative between $\psi = 0$ and

$\psi = \psi(0)$. If $V(\psi)$ for a given Mach number and temperature ratio T_e/T_i is negative for all ψ, then no steady shock solutions exist.

Isothermal Electrons

Bardotti and Segre[2] showed that for $T_e/T_i = 20$ and Maxwellian ions, the isothermal electron term e^{ψ} forced $V(\psi)$ to be negative for Mach numbers (M) based on the hot ion linear acoustic speed exceeding 1.07. Recall that, experimentally, shocks were produced up to Mach numbers of 1.5 and the Mach number-potential maximum relationship disagreed with the predictions of Bardotti and Segre.[2] We now investigate whether the turbulent modifications to $V(\psi)$ can bring the isothermal electron theory into better agreement with experiment.

First, note that the explicit turbulence term in (35) makes a positive definite contribution to $-V(\psi)$, as does e^{ψ}. Therefore, the turbulence term acts to lower the critical Mach number above which steady shock formation is impossible. The possibility remains, however that turbulent modifications to the ion distribution function might permit shocks at higher Mach numbers. We therefore construct a model for the reflected ions which maximize the turbulent modification of the ion distribution function.

To determine $\bar{n}_i(\psi)$ would require solving Eq. (16) for the ion distribution $\bar{f}_i$. However, the convecting wave turbulence resonantly interacts primarily with the reflected ions ($v_x < 0$) while the incident ions ($v_x > 0$) are only slightly affected by the waves. Therefore, a reasonable approximation for the incident ion distribution function $\bar{f}_>(v_x,x)$ is to assume that $\bar{f}_>$ is just the unperturbed upstream distribution. If we assume that $\bar{f}_>$ at $x = -\infty$ is a drifting Maxwellian, then after integration over v_y we can write

$$\bar{f}_{>}(v_x,x) = A \exp\left[\frac{1}{a_i^2}\left[(W_x)^{1/2} - u_0\right]^2\right] \tag{36}$$

where u_0 is the upstream flow speed (or shock speed in the laboratory frame), and A is a normalization constant to be determined.

The instability analysis of the truncated Maxwellian distribution indicates that the spatial growth rate is very large, especially in the shock front. Therefore, we would expect a very rapid turbulent relaxation of the reflected ion distribution $\bar{f}_{<}(w_x,x)$ to a marginally stable state, which would be well-approximated by a plateau in the velocity range where v_x is comparable to the unstable wave phase speeds ω/k_x. In a more exact treatment, resonance broadening would enhance the formation of a plateau, and permit diffusion to velocities exceeding the specular edge velocity $-v_0(x)$ of the unperturbed reflected Maxwellian.

Since ions with $v_x = 0$ should undergo little diffusion, the reflected and incident distributions will be equal at $v_x = 0$. If we assume that wave turbulence flattens $\bar{f}_{<}$ from $v_x = 0$ to a new edge velocity $-v_1(x)$ and that $\bar{f}_{<} \tilde{\simeq} 0$ for $v_x < -v_1(x)$, we can write

$$\bar{f}_{<}(W_x,x) = \bar{f}_{>}(v_x = 0,x) = \bar{f}_{>}[W_x = e\bar{\phi}(x)] \quad . \tag{37}$$

To determine $v_1(x)$, we can use the conservation of particle flux which is an exact consequence of Eq. (16). Steady state requires that the reflected ion flux $J_x(x)$ at each x be equal to the incident ion flux in the velocity range $0 \leq v_x \leq v_0(x)$, i.e., incident ions which will eventually reflect. $J_x(x)$ is given by

$$J_x(x) = \int_0^{v_0(x)} v_x \bar{f}_{>}(W_x)dv_x = \frac{1}{M_i}\int_{e\bar{\phi}(x)}^{e\bar{\phi}(0)} \bar{f}_{>}(W_x)dW_x \quad . \tag{38}$$

The reflected ion flux is

$$\int_{-v_1(x)}^{0} v_x \bar{f}_< dv_x = - \bar{f}_>[e\bar{\phi}(x)] \frac{v_1^2(x)}{2} = -J_x(x) \quad . \tag{39}$$

Whereupon

$$V_1(x) = \left[\frac{2}{M_i \bar{f}_>[e\bar{\phi}(x)]} \int_{e\bar{\phi}(x)}^{e\bar{\phi}(0)} \bar{f}_>(W_x) dW_x \right]^{1/2} \quad . \tag{40}$$

The incident ($\bar{n}_>$) and reflected ($\bar{n}_<$) ion densities are

$$n_>[e\bar{\phi}(x)] = \int_0^\infty dv_x \bar{f}_>(W_x)$$

$$\bar{n}_<[e\bar{\phi}(x)] = \left[\frac{2}{M_i} \bar{f}_>[e\bar{\phi}(x)] \int_{e\bar{\phi}(x)}^{e\bar{\phi}(0)} \bar{f}_>(W_x) dW_x \right]^{1/2} \quad . \tag{41}$$

If we set the upstream [$\bar{\phi}(x = -\infty) = 0$] ion density $\bar{n}_>(0) + n_<(0)$ equal to the upstream electron density $n_e(x = -\infty)$, and substitute (36) into (41), the normalization constant A is given by

$$A = \frac{2\bar{n}_e(-\infty)}{\sqrt{\pi}\, a} \left\{ 2 - \operatorname{erfc}\left(\frac{u_0}{a}\right) + \frac{2}{\sqrt{\pi}} \left[\exp\left(-\frac{u_o^2}{a^2}\right) \left(\exp\left(-\frac{u_0^2}{a^2}\right) - \right.\right.\right.$$

$$\left. - \exp\left(-\frac{1}{a^2} \left[\left(\frac{2e\bar{\phi}(0)}{M_i} \right)^{1/2} - u_0 \right]^2 \right) + \frac{u_0\sqrt{\pi}}{a} \left[\operatorname{erf}\left(\frac{u_0}{a}\right) - \operatorname{erf}\left\{ \frac{1}{a} \left(u_0 - \right.\right.\right.\right.$$

$$\left.\left.\left.\left.\left. - \left(\frac{2e\bar{\phi}(0)}{M_i} \right)^{1/2} \right\} \right] \right) \right] \right\}^{-1} \quad . \tag{42}$$

Equations (36) and (41) were substituted into (35) and the critical Mach number for $T_e/T_i = 20$ was determined as M = 1.1, or roughly identical to the

Bardotti and Segre[2] result. In this calculation the explicit turbulence term in (35) was neglected since the plateau distribution for the reflective ions already includes the maximal turbulent modification of the ion distribution function. Since this critical Mach number is well below the experimentally observed Mach numbers, we conclude that the experimental shocks are inconsistent with the theoretical assumption of isothermal electrons even when turbulent modification of the ion distribution functions is included.

Maximally Trapped Electrons

We now investigate the turbulent modifications to the theoretical shock structure predicted by the maximally trapped electron equation of state, Eq. (2). We replace the isothermal term e^{ψ} in (35) by $P(\psi)/P_0$ from (2) and solve for the Mach number as a function of the maximum potential $\psi(0)$. As a first approximation, we assume that the turbulence only slightly modifies the reflected ion distribution so that the M vs $\psi(0)$ relationship should only be slightly shifted from that computed assuming Maxwellian ions. If we expand $V(\psi)$ about the value of ψ_m determined by setting the first two terms in (35) equal to zero, the shift in the maximum potential $\Delta\psi = \psi(0) - \psi_m$ due to the explicit turbulence term in (35) is given by

$$-V(\psi_m+\Delta\psi) \cong -\left.\frac{\partial V}{\partial \psi}\right|_{\psi} \Delta\psi + \sum_{\omega} \frac{k_x^* k^2}{} \frac{\partial \mathrm{Re}\varepsilon}{\partial k_x} |\psi_\omega|^2 \left[\exp\left(-2\int_{-\infty}^{0} k_i dx'\right) - 1\right]$$

or

$$\Delta\psi \cong -\frac{\sum_{\omega} \frac{k_x^* k^2 \frac{\partial \mathrm{Re}\varepsilon}{\partial k_x} |\psi_\omega|^2_{max}}{2}}{e^{\psi_m} \operatorname{erfc}\sqrt{\psi_m} + \frac{2}{\sqrt{\pi}}\sqrt{\psi_m} - \frac{\bar{n}_>(\psi_m)}{\bar{n}_e(-\infty)}} \tag{43}$$

where $|\psi_\omega|^2_{max} = |\psi_\omega|^2 [\exp(-2 \int_{-\infty}^{0} k_i dx') - 1]$ is the maximum wave amplitude at $x = 0$ and $\bar{n}_>(\psi_m)$ is given by (41).

For $T_e/T_i = 20$ and Mach numbers $1.1 \leq M \leq 1.4$, the denominator in (43) is approximately -0.65. The maximum wave amplitudes observed in the experiments are on the order of $|\psi_\omega|_{max} \tilde{\approx} 10^{-1}$. From Eq. (24) it can be shown that $\partial Re\varepsilon/\partial k_x$ is approximately $\partial Re\varepsilon/\partial k_x \tilde{\approx} 2/k_x[1 + 2(k_x^2/k^2)] \tilde{\approx} 4/k_x$. For the oblique unstable ion waves $k \tilde{\approx} 1.5$, so that we obtain $\Delta\psi \tilde{\approx} 0.07$. Figure 15 shows the M vs $\psi(0)$ relation for both the Maxwellian ions without turbulence and the same curve shifted by $\Delta\psi = 0.07$. Since the $\Delta\psi$-shifted curve is in poorer agreement with experiments, we conclude that turbulent modification of the reflected ion distribution makes a significant change in the shock structure.

We also calculated the M vs $\psi(0)$ curve for the plateau reflected ion distribution derived above, maximally trapped electrons, $T_e/T_i = 20$, and neglecting the explicit turbulence term in (35). This result is also shown in Figure 15. From the agreement between the theoretical and experimental curves we conclude that the electron distribution in the experimental shocks should closely approximate the maximally trapped electron distribution and that the dominant effect of the wave turbulence on the shock structure is well represented by a flattened reflected ion distribution.

Beam Decay Distance

Finally, we estimate the spaital extent of the region in which the reflected ions interact strongly with the ion acoustic turbulence, which gives a measure of the turbulent shock thickness. Separating the reflected ion contribution from Eq. (32) and neglecting all contributions proportional to the reflected ion density $n_<$ except the kinetic term, we have

$$\frac{d}{dx}\left(n_< M_+ v_x^2\right) \approx \frac{n_< M_+ \langle v_x^2 \rangle}{L_B} \approx -\sum_\omega \frac{k_x k^2 k_i}{4\pi} \frac{\partial \mathrm{Re}\epsilon}{\partial k_x} \frac{T_e^2}{e^2} |\psi_\omega|^2_{max} \tag{44}$$

where L_B is an effective beam decay distance and ϕ_ω has been replaced by its maximum value. In dimensionless units (44) becomes

$$\frac{L_B}{\lambda_D} = \frac{n_<}{n_e} \frac{\langle v_x^2 \rangle}{c_s^2} \frac{1}{\sum_\omega k_x k^2 k_i \frac{\partial \mathrm{Re}\epsilon}{\partial k_x} |\psi_\omega|^2_{max}} \quad . \tag{45}$$

For typical experimental parameters $n_</n_e \approx 0.05$, $\langle v_x^2 \rangle \approx 4c_s^2$, $k_i \approx 0.1$, $|\psi_\omega|^2 \approx 10^{-2}$, and $k = 1.5$, we find $L_B/\lambda_D \approx 20$, in rough agreement with experimentally observed values of the spatial extent of the wave turbulence region.

VI. SUMMARY

Electrostatic ion acoustic shock experiments in the University of California, Los Angeles, double plasma device have revealed three distinct types of shock structures. 1) A laminar shock with a trailing wave train of potential oscillations in which few ions are reflected from the shock potential jump; 2) a weakly turbulent shock in which the reflected ion-driven ion acoustic turbulence is confined ahead of the major jump in shock potential; 3) a more strongly turbulent shock in which the ion acoustic turbulence propagates throughout the shock front and has amplitudes comparable to the steady shock potential. In the first two types of shocks, the potential jump is sharp occurring on scale lengths of a few Debye lengths; for the third type of shock, the shock transition is considerably broader, and occurs on scale lengths on the order of the reflected ion decay distance, some tens of Debye lengths. The unstable ion acoustic waves are believed to propagate at large angles to the shock normal. Figure 16 presents a qualitative summary of the shock in terms of the parameter range of the experiments. The boundaries between the small and large amplitude turbulent shocks are not precise. Also recall that the shock evolves from one state to another as it propagates away from the formation region.

For T_e/T_i in the range 10 to 40, shocks with Mach numbers between 1.05 and 1.5 have been observed. These Mach numbers generally exceed the maximum Mach number calculated by Bardotti and Segre[2] for isothermal electrons and Maxwellian ions. Steady state shock calculations assuming trapped electrons[6] and turbulently flattened reflected ions predict a Mach number vs maximum shock potential relationship which agrees well with experiment. This agreement suggests that in the double plasma shock experiments the electrons are indeed trapped in the steady shock potential. Electrons could become trapped between the

negatively biased excitation grid and the shock front, and execute several bounces in this effective potential well before colliding with the side chamber walls. Hence, the existence of a flat-topped distribution of trapped electrons in these experiments is probably reasonable. Indeed such a trapped-electron distribution was recently observed (in another UCLA DP device) in the potential maxima of current-driven ion acoustic waves of large amplitude $\left(\frac{n_1}{n_o} \gtrsim 102\right)$.[22]

The difference between the two types of turbulent shocks is not currently understood. The weakly turbulent shocks appear to require that the unstable ion acoustic waves be close to group standing in the shock front. The linear instability theory of a Maxwellian ion beam plasma indicates that the group standing condition might be satisfied, although a parametric investigation of the group standing condition is prohibited by our imprecise knowledge of the reflected ion distribution functions and the angular distribution of the unstable waves. If the waves have an approximately zero group velocity in the shock frame, then wave saturation becomes an interesting theoretical and experimental problem. Since in steady state these waves would be continuously driven unstable by the reflected ions, wave saturation could occur by mode coupling to non-group standing waves, as in the early perpendicular magnetosonic whistler shock theory of Camac et al.[23] Alternatively, if the waves propagated slightly faster than the shock front, the waves might simply damp out ahead of the shock. A more detailed experimental and theoretical investigation is needed to clarify these points.

In the strongly turbulent shocks, ions are no longer reflected by a smooth laminar potential barrier but by a spatially and temporally turbulent shock potential. Hence, the essentially laminar theory, which was used in this paper, is probably inadequate to accurately describe the shock structure, and effects such as ion trapping in the shock front must be considered. At what point the essentially fluid shock description with superimposed wave turbulence goes over into the fully turbulent kinetic shock description remains to be resolved.

Acknowledgments

It is a pleasure to acknowledge many beneficial discussions with Professors B. D. Fried, C. F. Kennel, and K. MacKenzie, and Drs. R. J. Taylor, H. Ikezi, and P. Barrett.

This work was partially supported by the Office of Naval Research, Grant #N00014-69-A-0200-4023; the National Science Foundation, Grant # GP-22817; the Atomic Energy Commission, Contract AT(04-3)-34, Project #157; and the National Aeronautics and Space Administration, Contract NGL-05-007-190.

References

1. S. S. Moiseev and R. Z. Sagdeev, J. Nucl. Energy, Pt. C5, 43 (1962); R. Z. Sagdeev, in Reviews of Plasma Physics, edited by M. A. Leontovich (Consultants Bureau, New York, 1966), Vol. 4.
2. G. Bardotti and S. E. Segre, Plasma Phys. 12, 247 (1970).
3. D. Montgomery, Phys. Rev. Letters 19, 1465 (1967).
4. D. Montgomery and G. Joyce, J. Plasma Phys. 3, 1 (1969).
5. I. B. Bernstein, J. M. Greene, and M. D. Kruskal, Phys. Rev. 108, 546 (1957).
6. D. W. Forslund and J. P. Freidberg, Phys. Rev. Letters 27, 1189 (1971).
7. D. W. Forslund and C. R. Shonk, Phys. Rev. Letters 25, 1699 (1970).
8. D. A. Tidman, Phys. Fluids 10, 547 (1967).
9. R. J. Taylor, D. R. Baker, and H. Ikezi, Phys. Rev. Letters 24, 206 (1970).
10. A. Y. Wong and R. W. Means, Phys. Rev. Letters 27, 973 (1971); R. W. Means and A. Y. Wong, Bull. Am. Phys. Soc. 15, 1409 (1970).
11. R. A. Stern and J. F. Decker, Phys. Rev. Letters 27, 1266 (1971).
12. J. W. M. Paul et al., Am. Phys. Soc. 16, 1191 (1971); P. E. Phillips and A. E. Robson, Phys. Rev. Letters 20, 154 (1972); I. M. Podgorny, Y. V. Andrianov, and E. M. Dubinin, XV Meeting of CosPAR, Madrid, Spain (1972).
13. A. E. Robson, Collision-Free Shocks in the Laboratory and Space, ESRO SP-51, 159 (1969).
14. R. J. Taylor, Ph.D.Thesis, University of California, Los Angeles (1970).
15. D. B. Cohn and K. MacKenzie, Phys. Rev. Letters 28, 656 (1972).
16. The Mach number of this shock wave was erroneously published as 1.05 in Ref. 10. The correct Mach number is 1.2.
17. R. J. Taylor and F. V. Coroniti, Phys. Rev. Letters 29, 34 (1972).
18. P. H. Sakanaka, Phys. Fluids 15, 304 (1972); P. H. Sakanaka, C. K. Chu, and T. C. Marshall, Phys. Fluids 14, 611 (1971).

19. R. J. Mason, Phys. Fluids 13, 1042 (1970).

20. Turbulent structures were observed in computer simulation of a plasma with 10% light ions. D. W. Forslund (private communication).

21. B. D. Fried and A. Y. Wong, Phys. Fluids 9, 1084 (1966).

22. A. Y. Wong, B. H. Quon and B. H. Ripin, UCLA, PPG-147, April 1973.

23. M. Camac, A. R. Kantrowitz, M. M. Litvak, R. M. Patrick, and H. E. Petschek, Nucl. Fusion Suppl., Pt. 2, 423 (1962).

Figure Captions

Fig. 1: Laminar shock profile of electron density $\Delta N/N$ vs time as a function of distance x from the separation grid of the DP device. The foot structure and reflected ions can be seen ahead of the sharp jump in electron density. Downstream of the shock density jump there is a trailing wave train of density oscillations. $M = 1.13$, $T_e/T_i = 13$, $V_b/C_s = 1.6$.

Fig. 2: Mach number M vs maximum shock potential $e\phi/T_e$. The crosses are experimental points for shocks with $5 \leq T_e/T_i \leq 50$. The solid curve is the average of the experimental points $M = 1.0 + 0.6\ e\phi/T_e$. The lower dashed curve is computed from the isothermal-cold-ion Sagdeev-Moiseev theory. The upper dashed curve is computed using the trapped electron equation of state with cold ions.

Fig. 3: Mach number M vs maximum shock potential $e\phi/T_e$ calculated using the trapped electron equation of state and a Maxwellian ion distribution for the incident ions and a truncated Maxwellian for the reflected ions.

Fig. 4: The density of ions reflected from the shock front n_b/n_0 vs the maximum shock potential $e\phi/T_e$ for $T_e/T_i = 10$ and 30. The reflected ion density predicted from a truncated Maxwellian reflected ion distribution and the experimental M vs the maximum $e\phi/T_e$ is shown as the solid line. The reflected ion density predicted by the Sagdeev-Moiseev M vs the maximum $e\phi/T_e$ is shown as the dashed line.

Fig. 5: The reflected ion density mean velocity V_b/C_s vs the maximum shock potential $e\phi/T_e$ for $5 \leq T_e/T_i \leq 50$. The solid curves were calculated assuming a truncated Maxwellian for the reflected ion distribution and the experimental average Mach number maximum shock potential relation.

Fig. 6: The electron density $\Delta N/N$ vs time as a function of distance x from the separation grid for a small amplitude turbulent shock. The turbulence appears as the blurred region. $M = 1.2$, $V_b/C_s = 1.8$, $T_e/T_i = 10$, $n_b/n_0 = 0.08$.

Fig. 7: The electron density $\Delta N/N$ vs time as a function of distance x from the separation grid for a large amplitude turbulent shock. $M = 1.2$, $V_b/C_s = 2.0$, $T_e/T_i = 16$, $n_b/n_0 = 0.05$.

Fig. 8: Individual large amplitude turbulent shock electron density profiles vs time. Each oscilloscope trace consists of three shock profiles taken at the same distance from the DP separation grid. The shock parameters are the same as Fig. 7.

Fig. 9: Continuation of Fig. 8 for further distances from the separation grid.

Fig. 10: The density ratio n(x) defined as the local shock electron density jump normalized to the initial shock electron density jump at $x = 2$ vs distance x.

Fig. 11: The angle θ to the direction of the ion beam at which unstable ion acoustic waves are detected vs the ion beam energy $e\phi_b/T_e$. The cross-hatched region represents a 3 db width in the power spectrum. The two solid curves represent approximate theoretical stability limits.

Fig. 12: The maximum spatial growth increment k_i/k_D for ion acoustic waves as a function of beam density n_b/n_0 for various T_e/T_i ratios. The beam velocity is 1.0 C_s.

Fig. 13: The group velocity V_g/C_s in the direction of the ion beam vs frequency ω/ω_{pi}. The lower curve is calculated neglecting the beam contribution to the group velocity; the upper curve includes the beam contribution.

Fig. 14: The spatial growth increment Im k_x vs potential $e\phi(x)/T_e$ in the shock front.

Fig. 15: Mach number M vs the maximum $e\phi/T_e$. The dashed curve is calculated with the electron equation of state and a truncated Maxwellian for the reflected ions; $T_e/T_i = 20$. The lowest curve is the dashed curve shifted by $\Delta(e\phi/T_e) = \Delta\psi = 0.07$. The average experimental M vs $e\phi/T_e$ relationship is shown as the top curve. The intermediate curve is calculated assuming trapped electrons and turbulently flattened reflected ions.

Fig. 16: Schematic summary of experimental shock results presented in a maximum shock potential vs T_e/T_i parameter space. The boundaries between the various types of observed shocks are not precise.

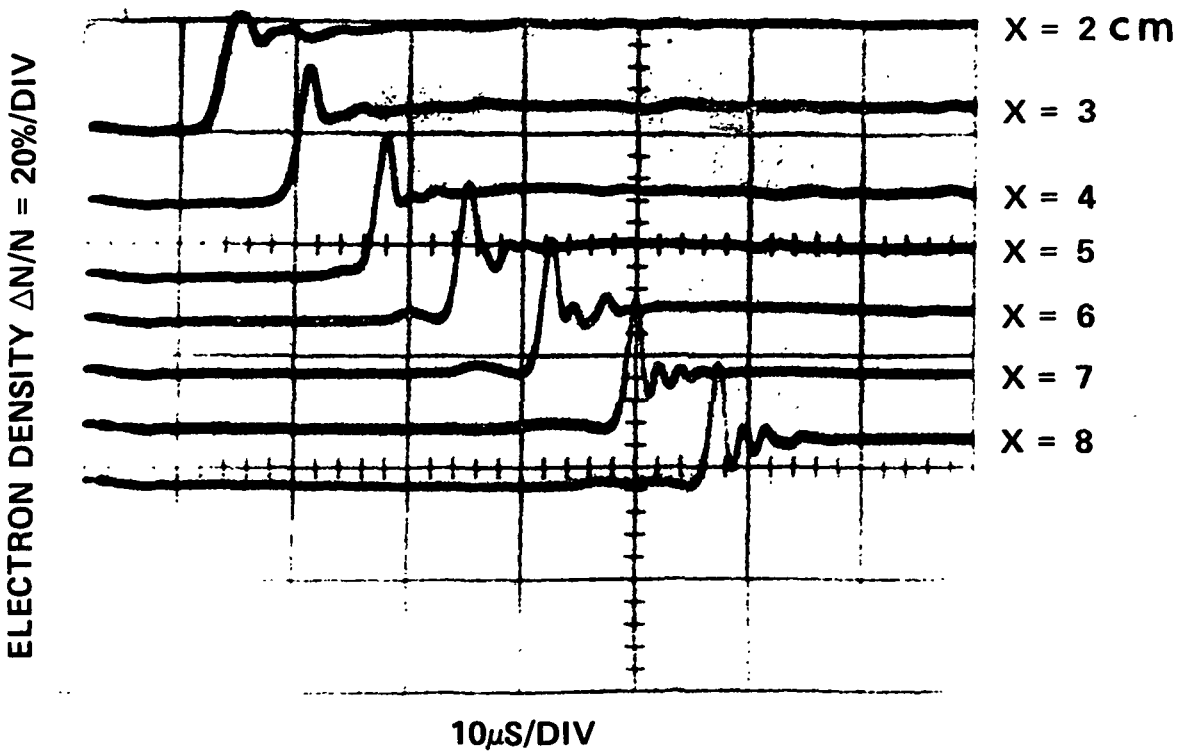
X = 2 cm
X = 3
X = 4
X = 5
X = 6
X = 7
X = 8
ELECTRON DENSITY ΔN/N = 20%/DIV
10μS/DIV

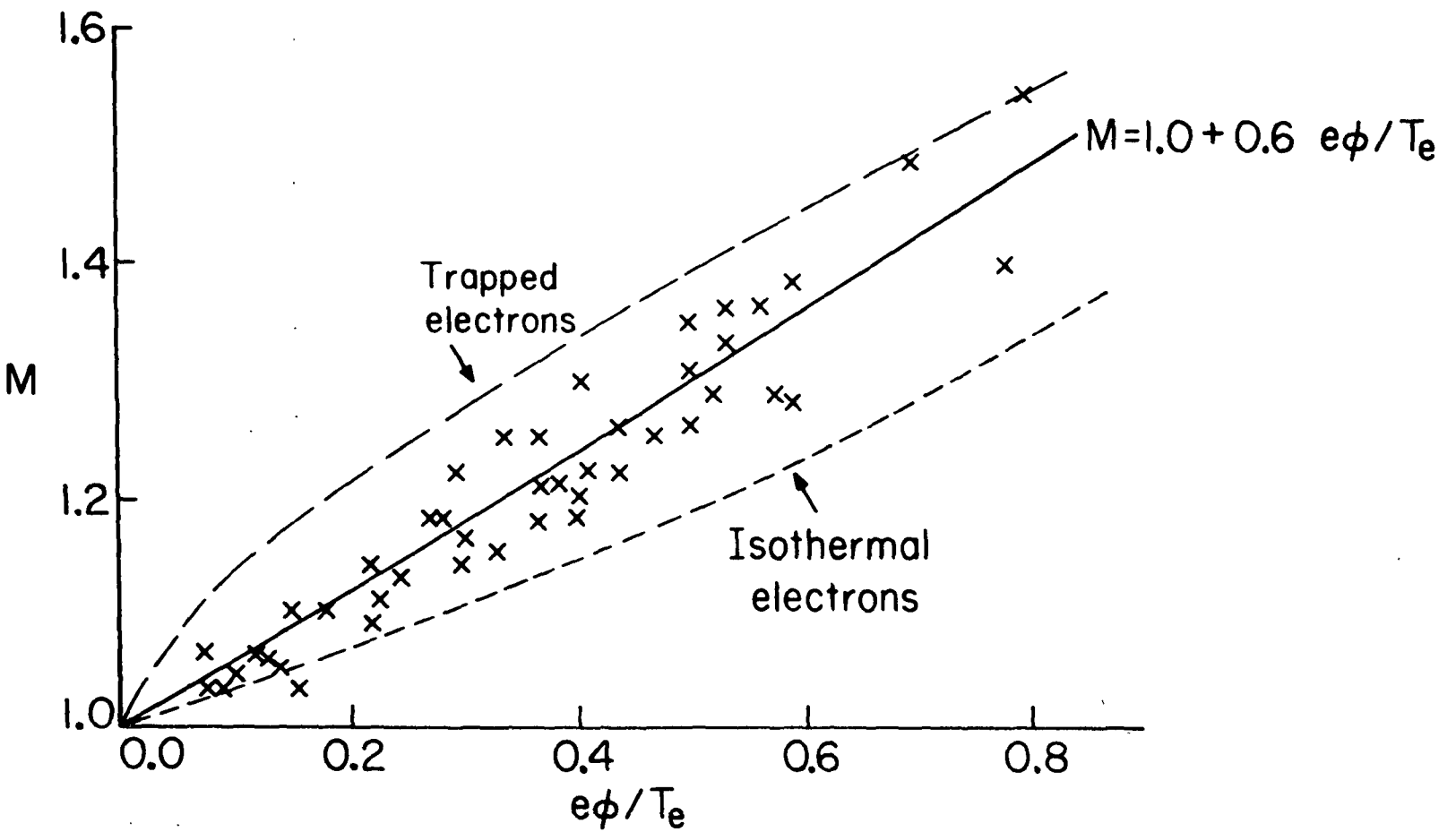
1.6
1.4
1.2
1.0
M
0.0
0.2
0.4
0.6
0.8
eϕ/Te
M=1.0+0.6 eϕ/Te
Trapped electrons
Isothermal electrons

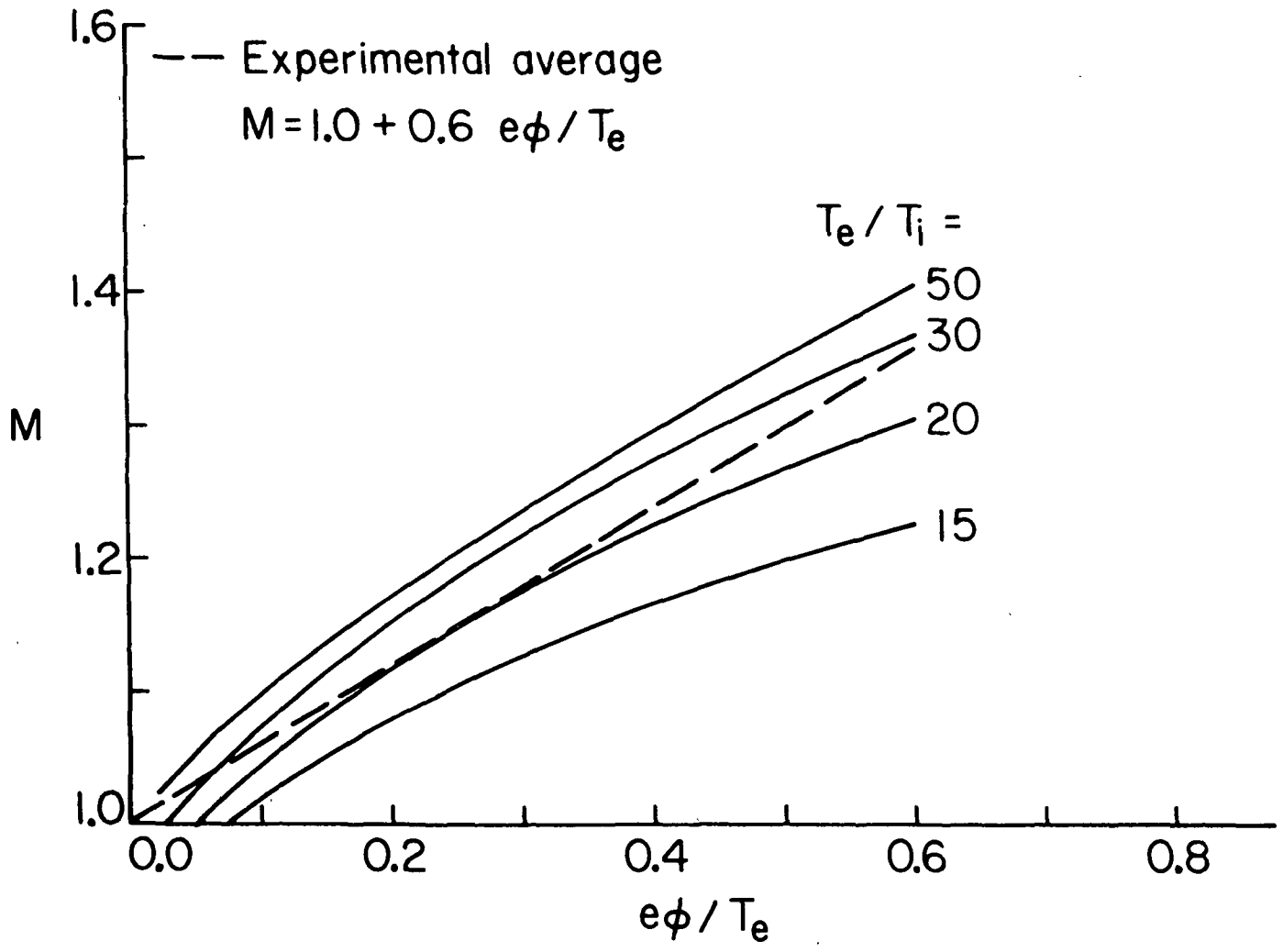
1.6
1.4
1.2
1.0
M
— — Experimental average
M = 1.0 + 0.6 eφ / Te
Te / Ti =
50
30
20
15
0.0
0.2
0.4
0.6
0.8
eφ / Te

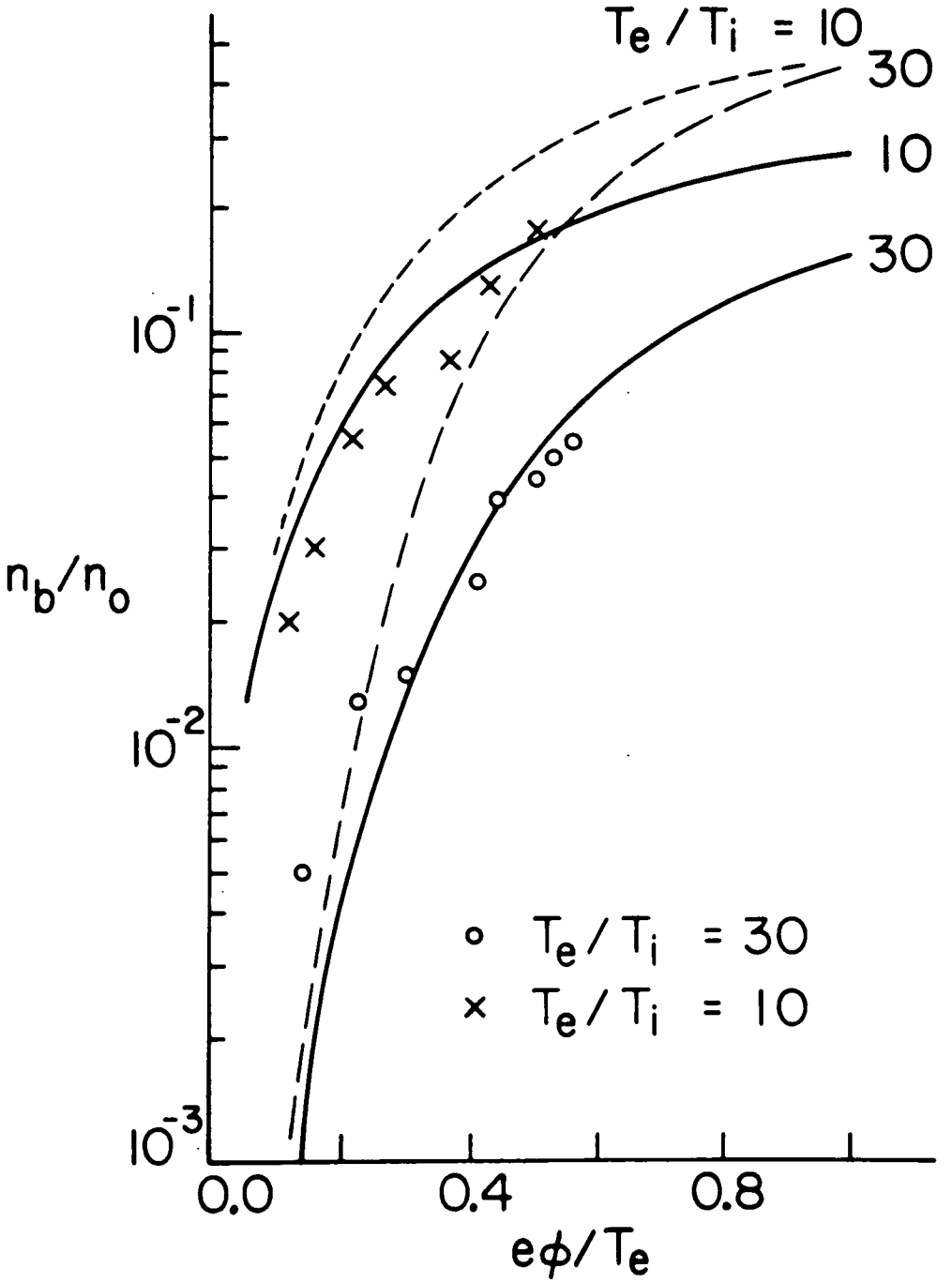
T_e / T_i = 10
30
10
30
10^{-1}
10^{-2}
10^{-3}
n_b/n_o
o T_e / T_i = 30
× T_e / T_i = 10
0.0
0.4
0.8
$e\phi/T_e$

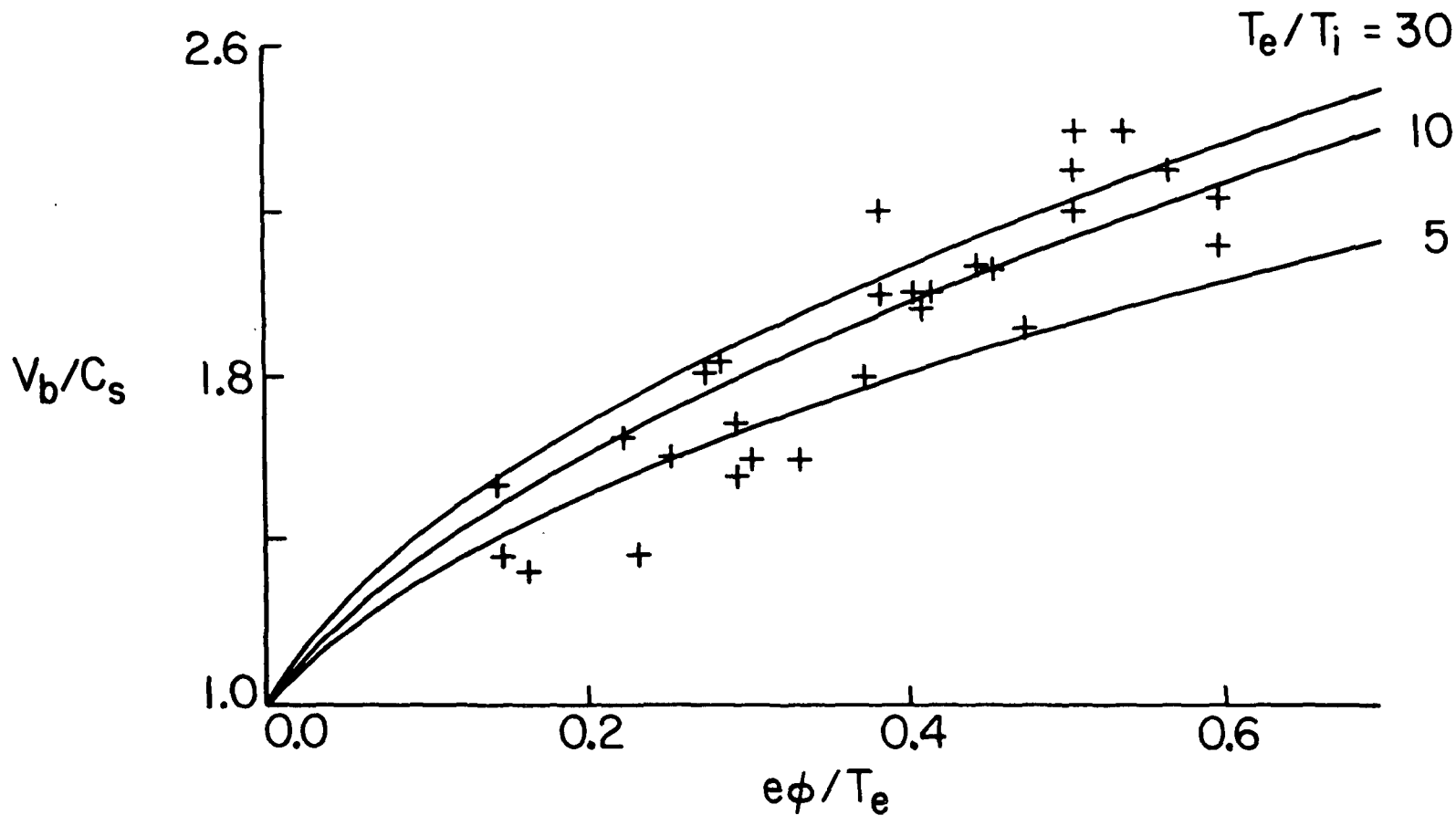
2.6
1.8
1.0
V_b/C_s
0.0
0.2
0.4
0.6
$e\phi/T_e$
$T_e/T_i = 30$
10
5

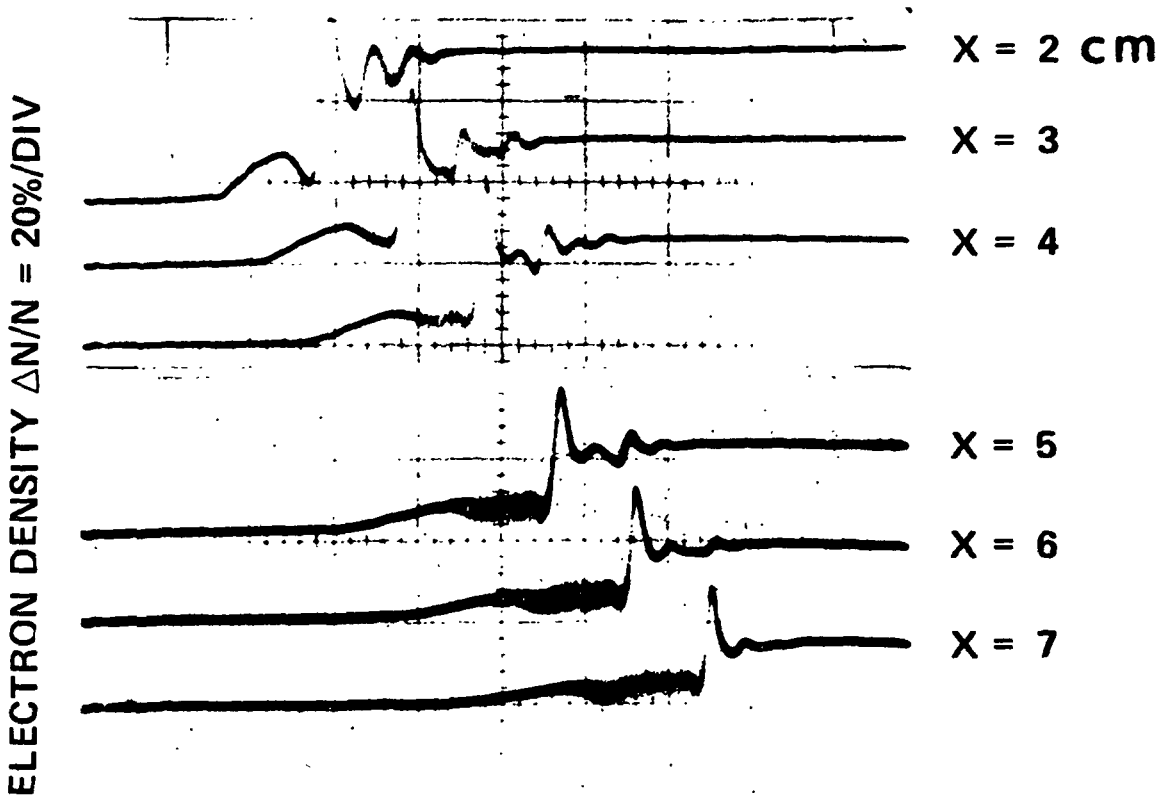
X = 2 cm
X = 3
X = 4
X = 5
X = 6
X = 7
ELECTRON DENSITY ΔN/N = 20%/DIV
10μS/DIV

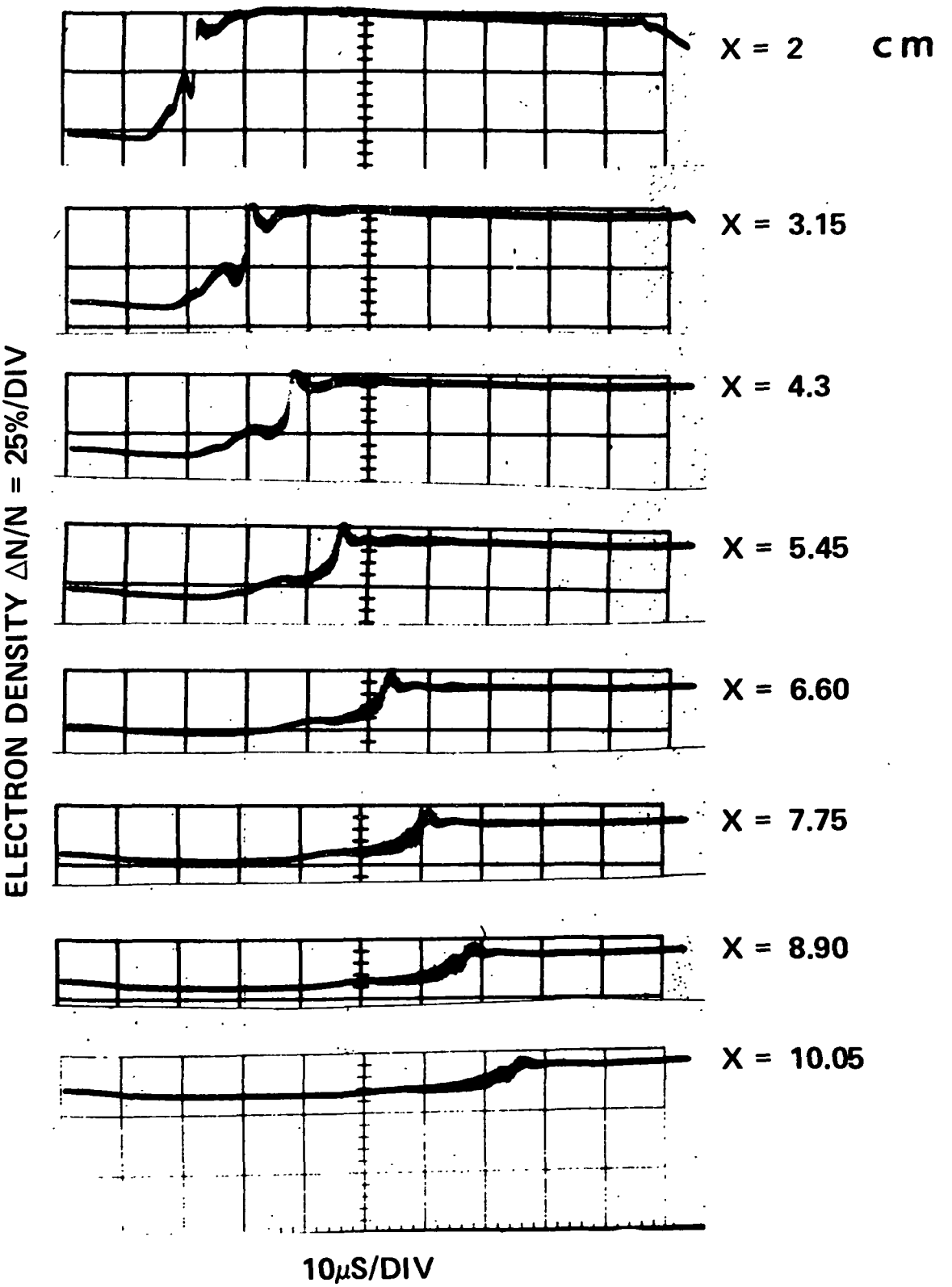
X = 2 cm
X = 3.15
X = 4.3
X = 5.45
X = 6.60
X = 7.75
X = 8.90
X = 10.05
ELECTRON DENSITY ΔN/N = 25%/DIV
10μS/DIV

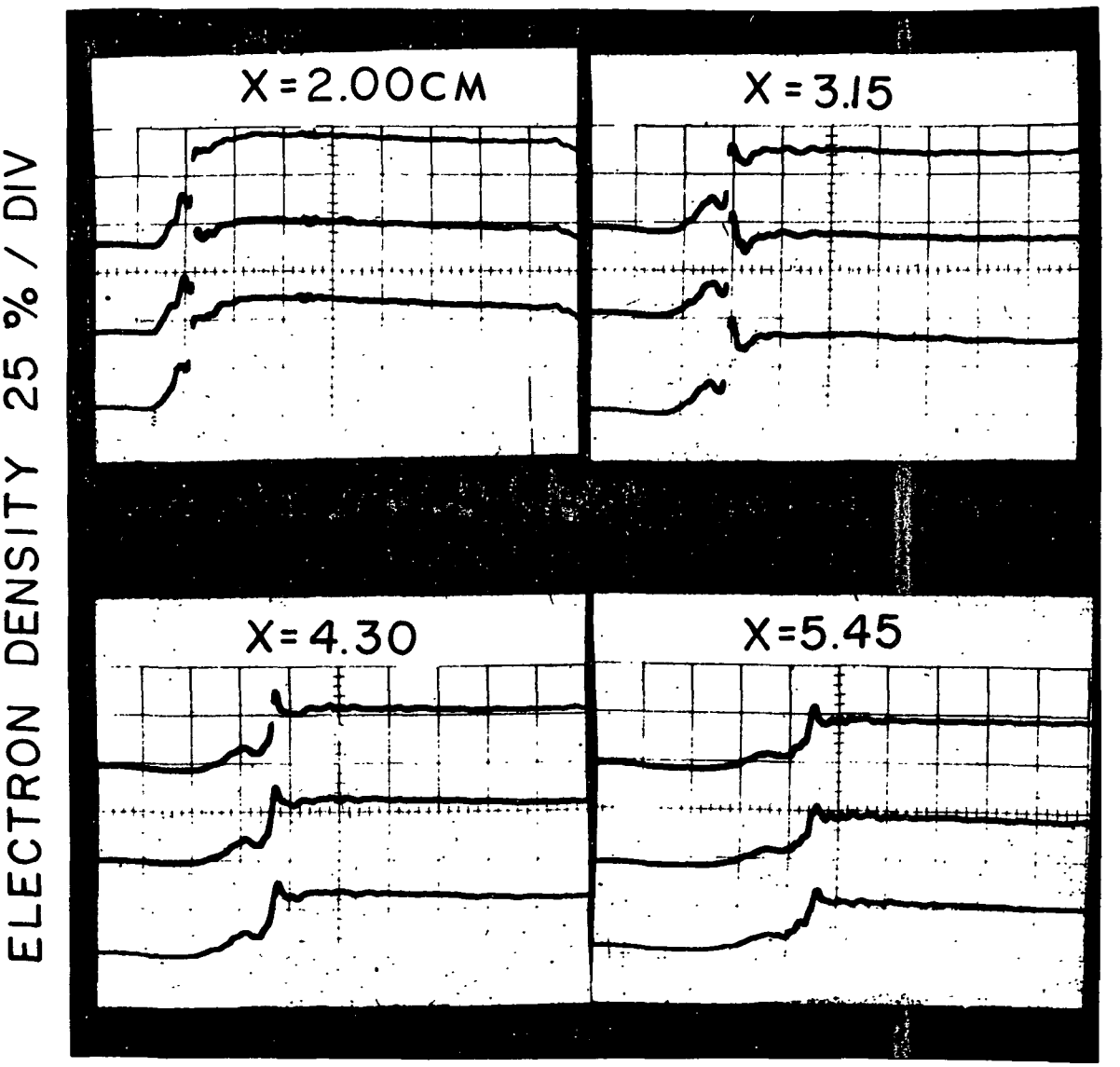
X = 2.00CM
X = 3.15
X = 4.30
X = 5.45
ELECTRON DENSITY 25 % / DIV
10 μS / DIV

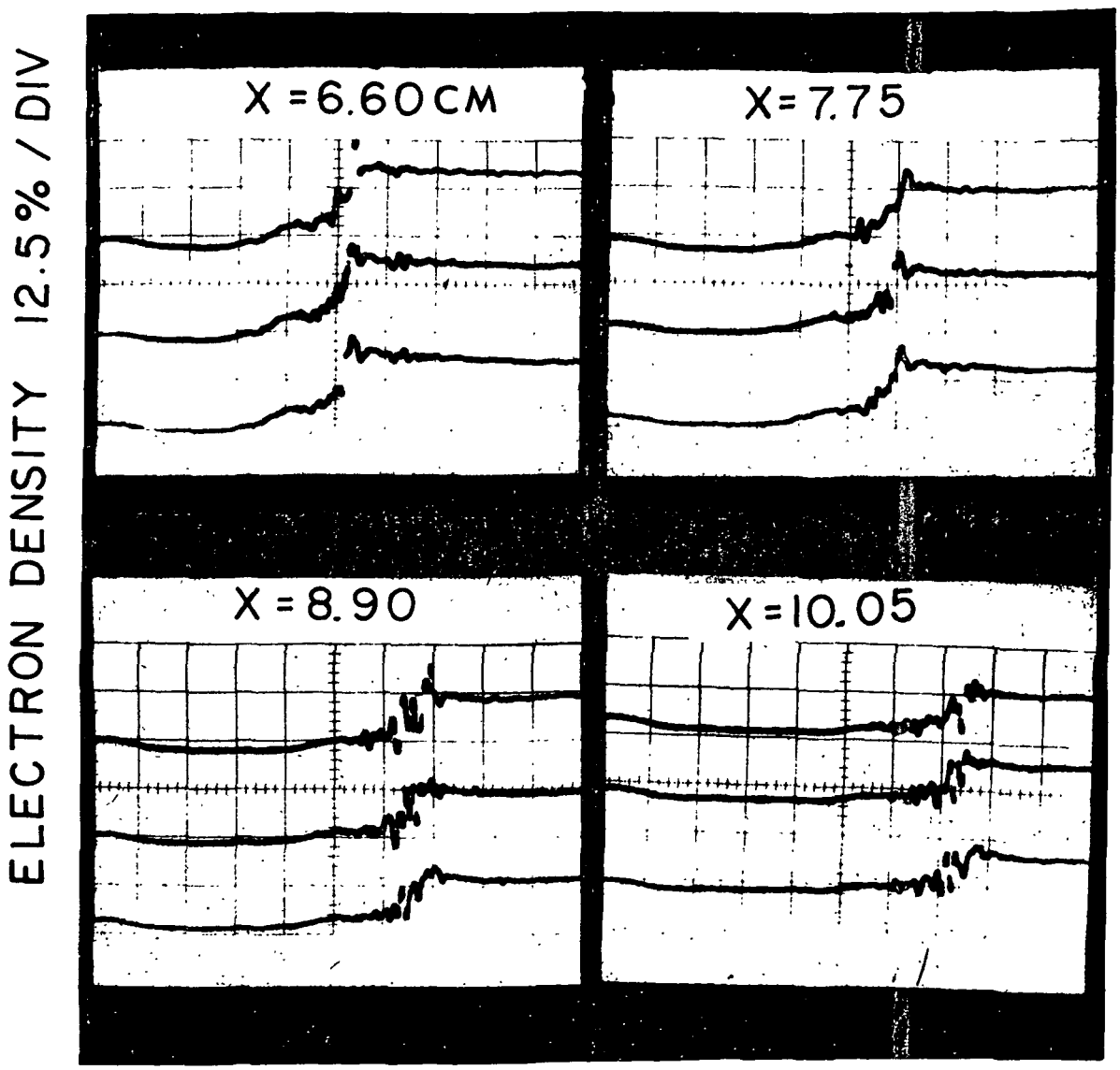
X = 6.60 CM
X = 7.75
X = 8.90
X = 10.05
ELECTRON DENSITY 12.5% / DIV
10 μS / DIV

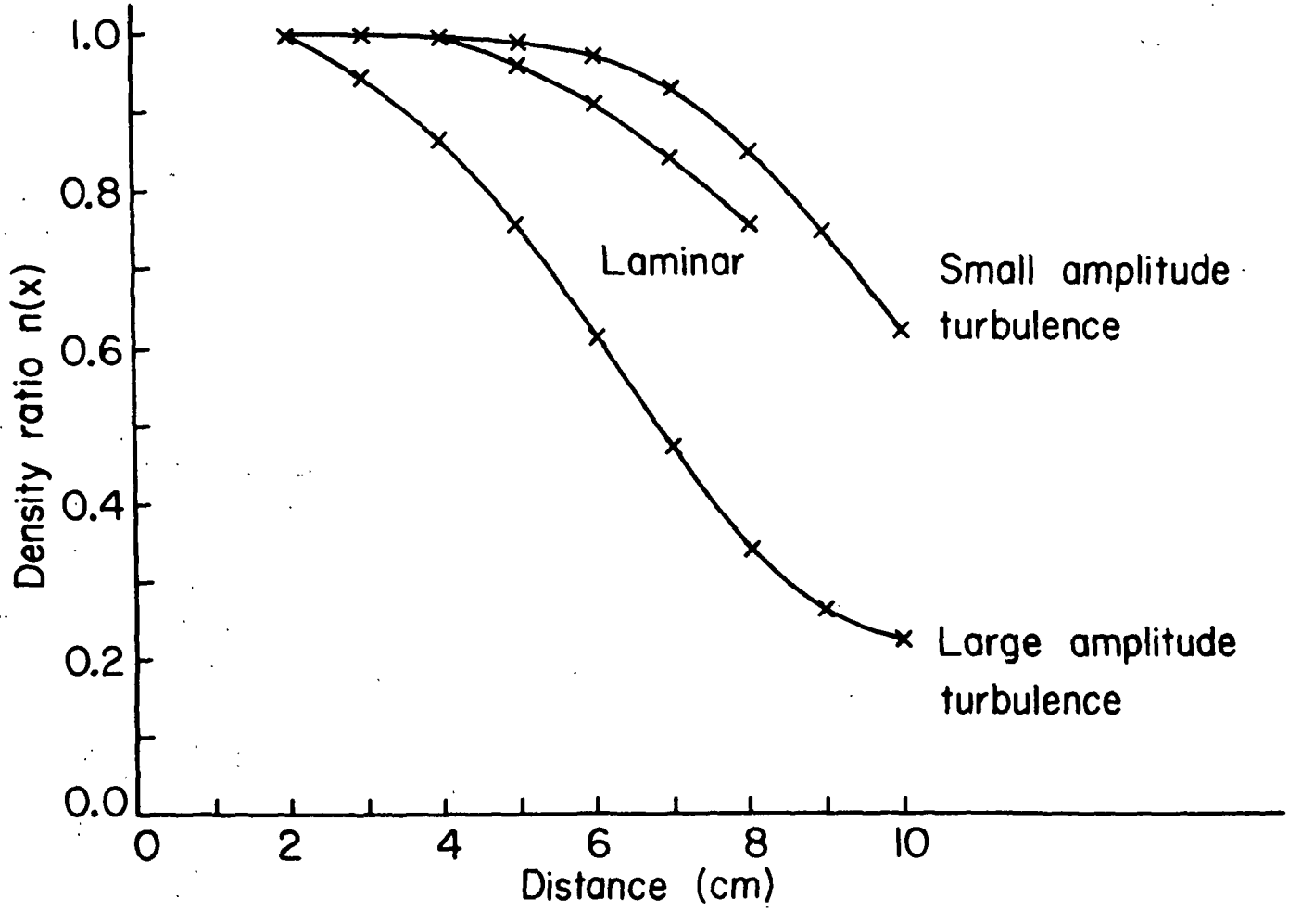
1.0
0.8
0.6
0.4
0.2
0.0
Density ratio n(x)
0
2
4
6
8
10
Distance (cm)
Laminar
Small amplitude turbulence
Large amplitude turbulence

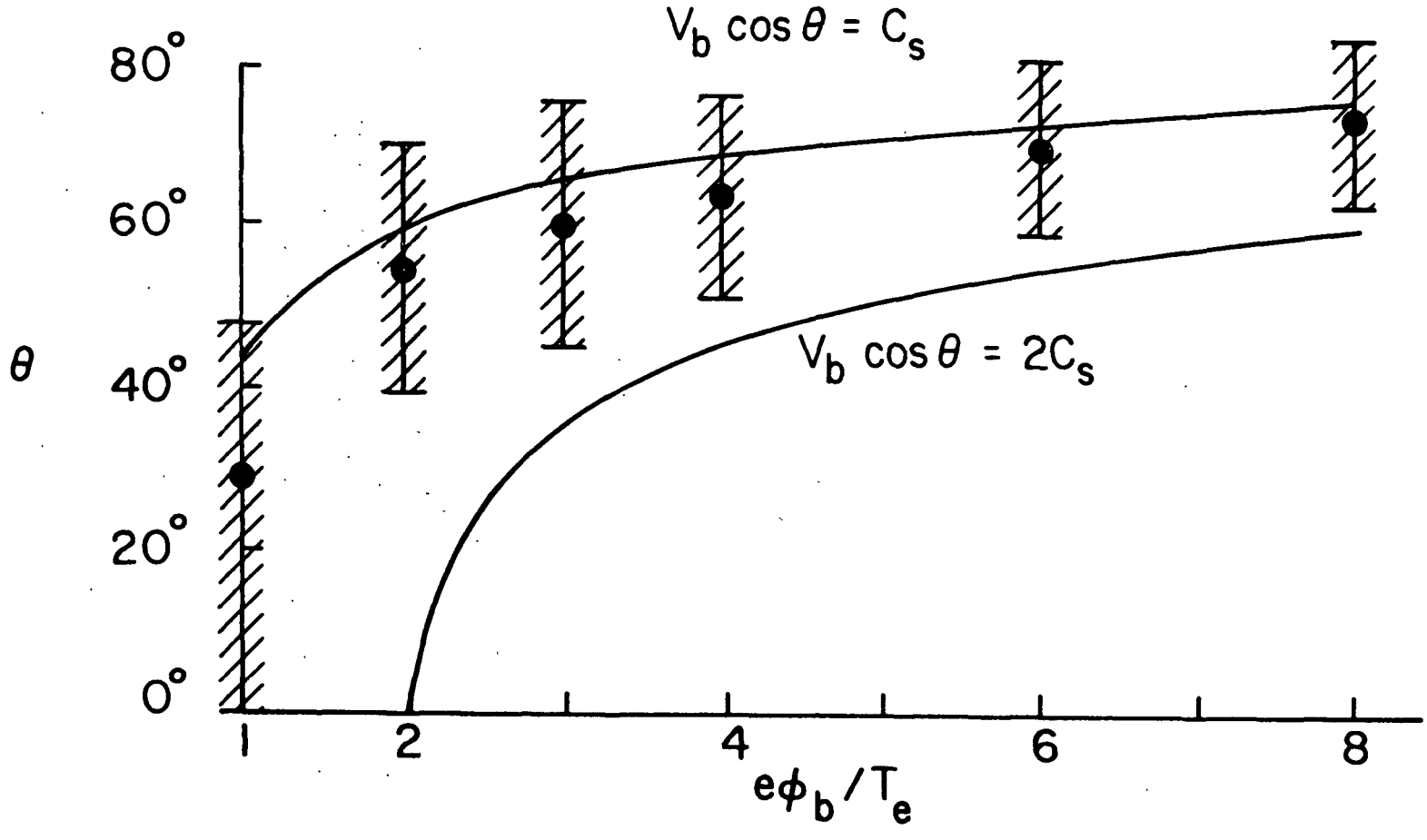
$V_b \cos\theta = C_s$
$V_b \cos\theta = 2C_s$
80°
60°
40°
20°
0°
θ
1
2
4
6
8
$e\phi_b / T_e$

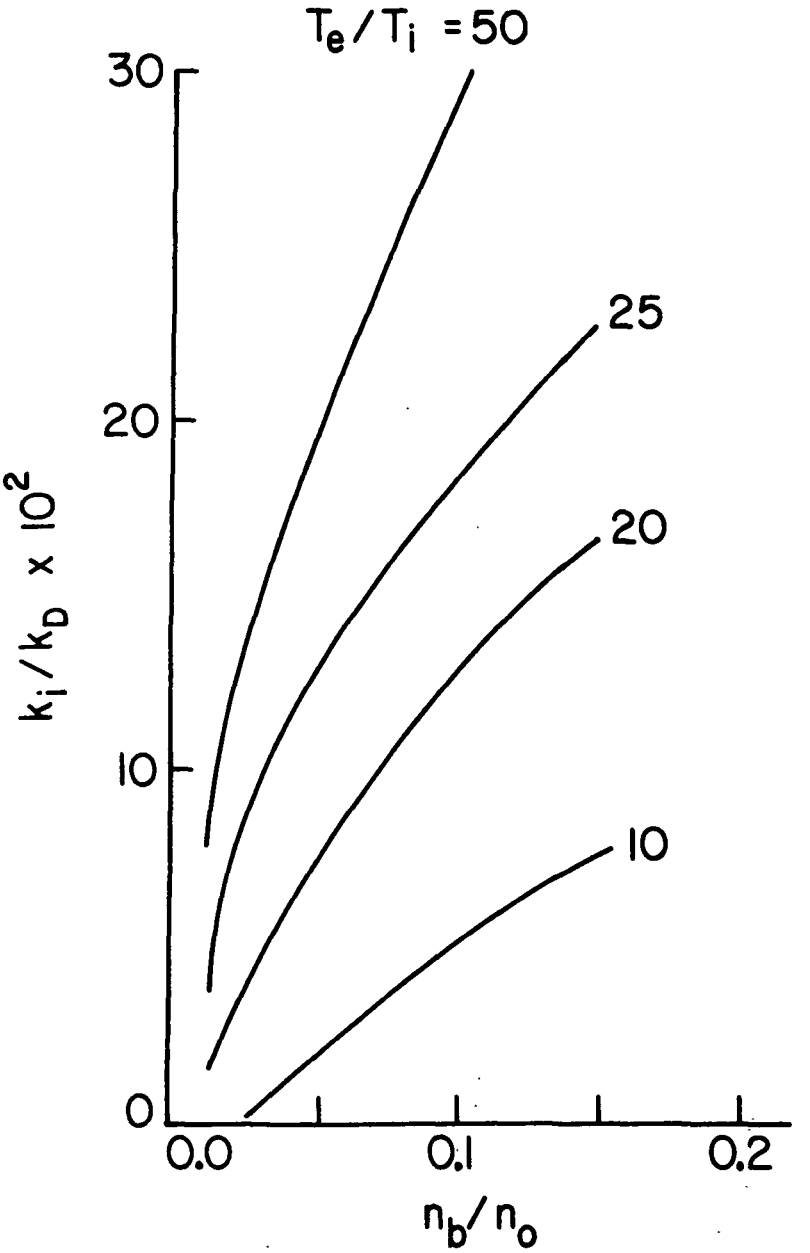
$T_e/T_i = 50$
25
20
10
30
20
10
0
$k_i/k_D \times 10^2$
0.0
0.1
0.2
n_b/n_o

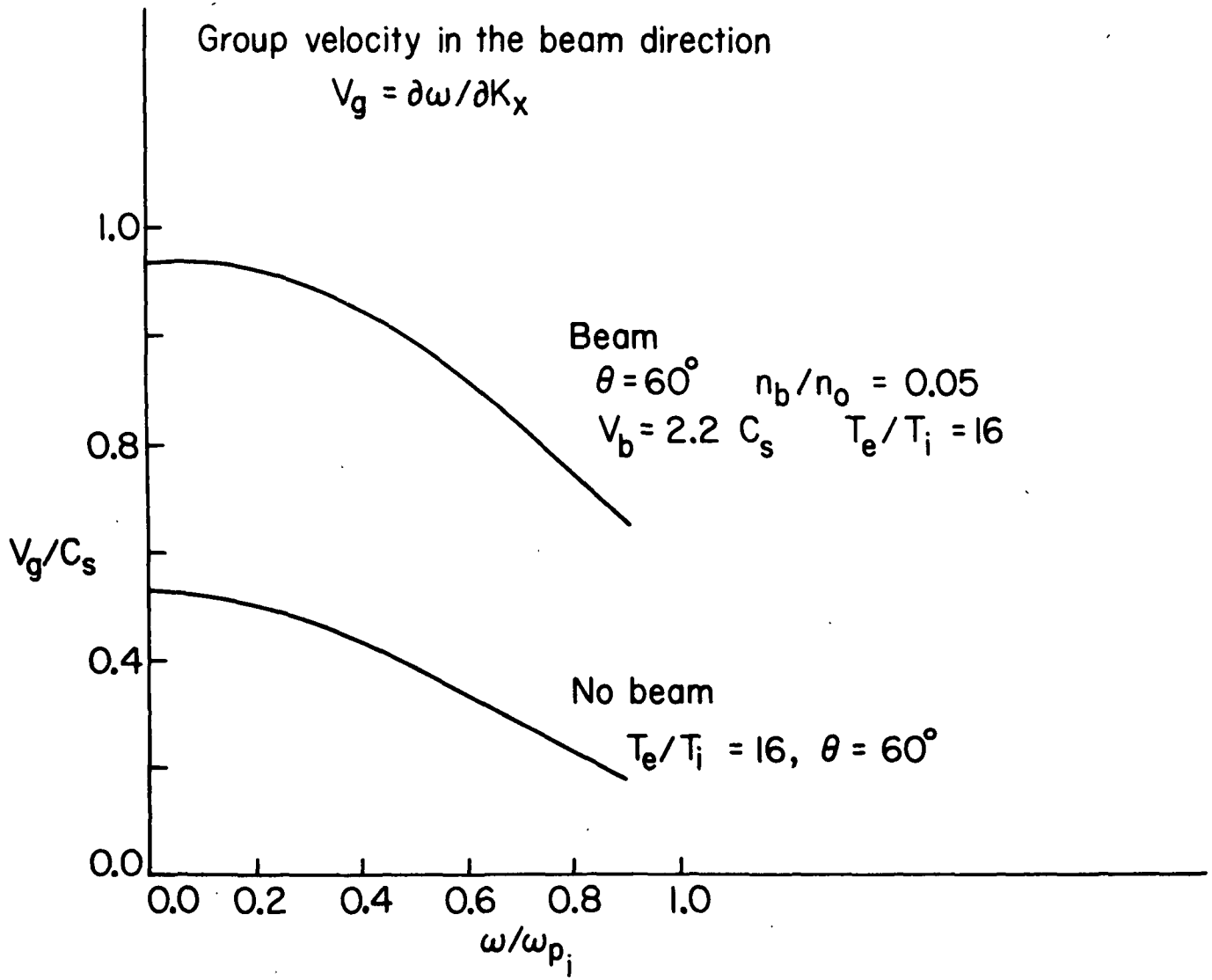
Group velocity in the beam direction
$V_g = \partial\omega/\partial K_x$
1.0
0.8
0.4
0.0
V_g/C_s
Beam
$\theta = 60^\circ$ $n_b/n_o = 0.05$
$V_b = 2.2\ C_s$ $T_e/T_i = 16$
No beam
$T_e/T_i = 16,\ \theta = 60^\circ$
0.0 0.2 0.4 0.6 0.8 1.0
ω/ω_{p_i}

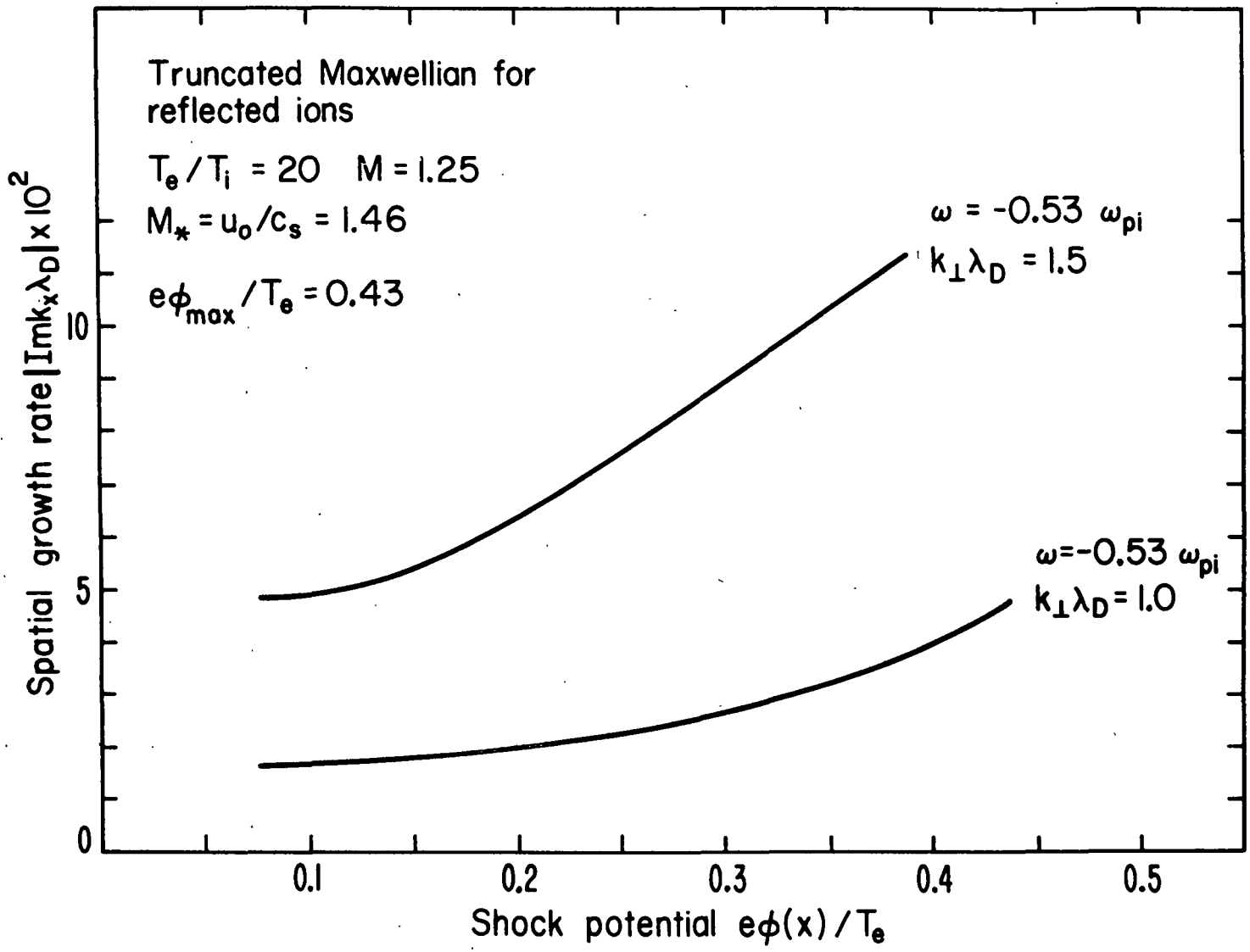
Truncated Maxwellian for
reflected ions
$T_e/T_i = 20$ $M = 1.25$
$M_* = u_o/c_s = 1.46$
$e\phi_{max}/T_e = 0.43$
$\omega = -0.53\ \omega_{pi}$
$k_\perp\lambda_D = 1.5$
$\omega = -0.53\ \omega_{pi}$
$k_\perp\lambda_D = 1.0$
Spatial growth rate $|Imk_x\lambda_D| \times 10^2$
0
5
10
0.1
0.2
0.3
0.4
0.5
Shock potential $e\phi(x)/T_e$

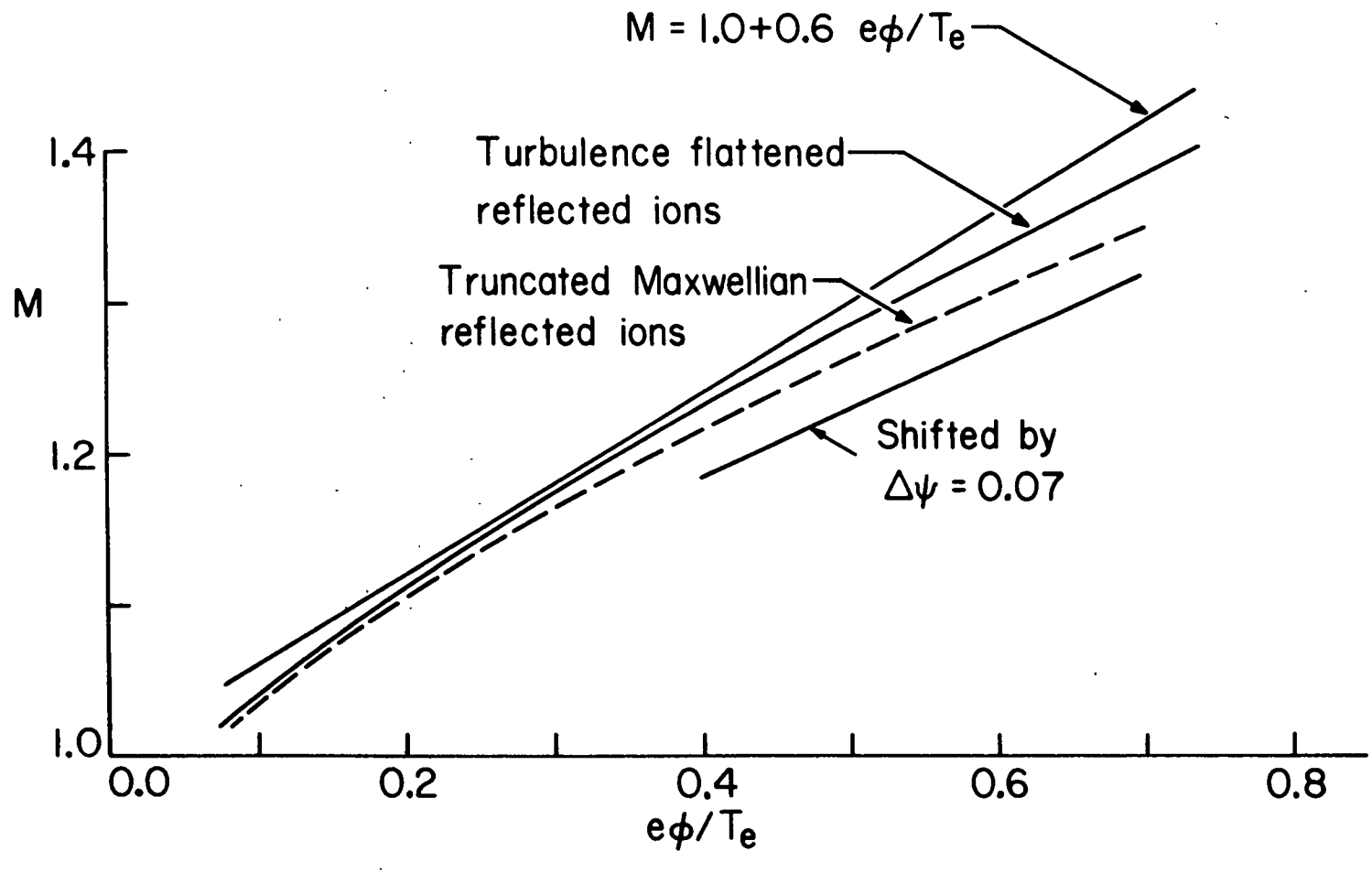
M = 1.0+0.6 eφ/Te
Turbulence flattened
reflected ions
Truncated Maxwellian
reflected ions
Shifted by
Δψ = 0.07
M
1.4
1.2
1.0
0.0
0.2
0.4
0.6
0.8
eφ/Te

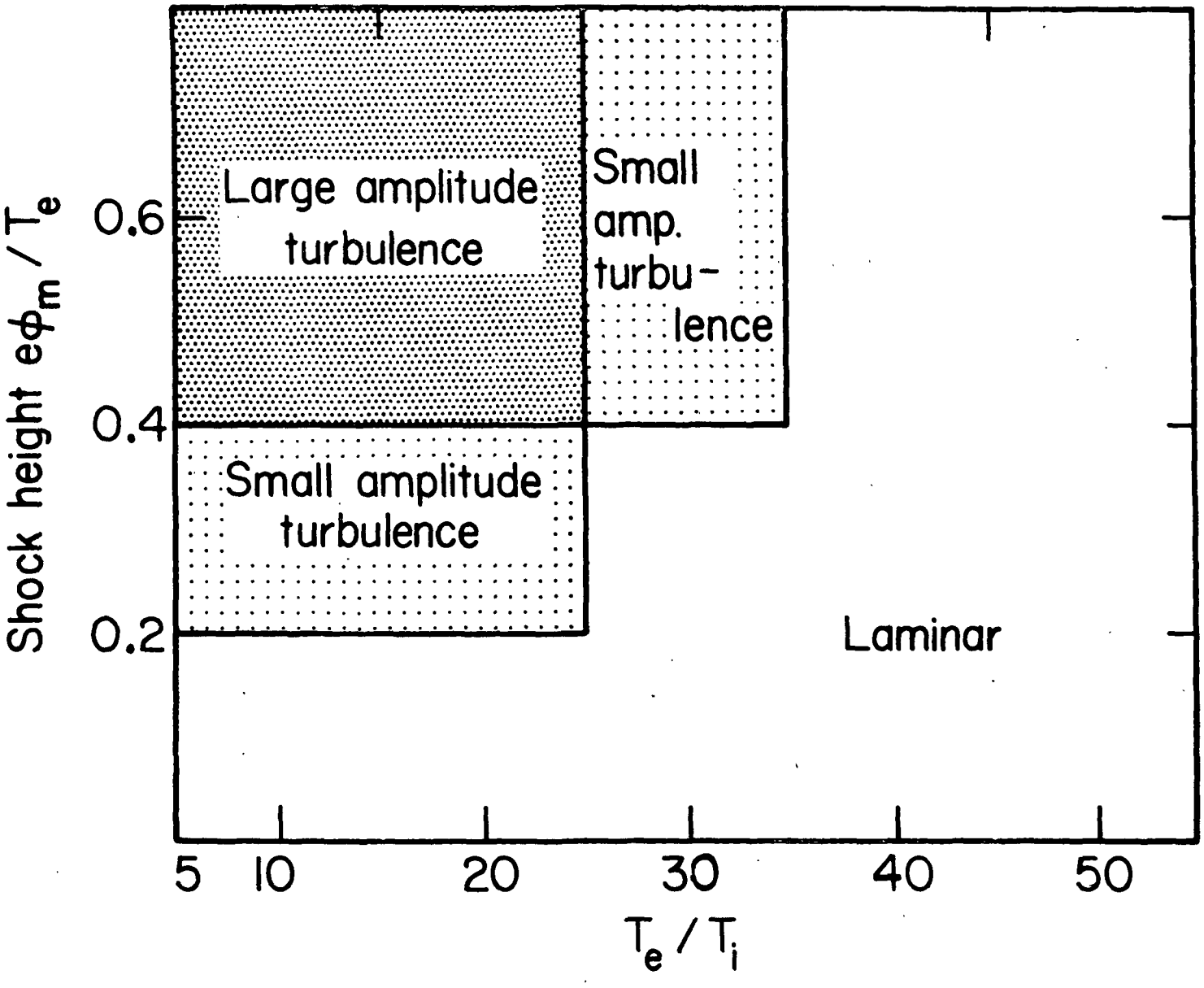
Large amplitude turbulence
Small amp. turbu- lence
Small amplitude turbulence
Laminar
Shock height $e\phi_m / T_e$
0.6
0.4
0.2
5
10
20
30
40
50
T_e / T_i

UCLA PLASMA PHYSICS GROUP REPORTS

* Published by Experimental Group
† Published by Theoretical Group

R-1 "Propagation of Ion Acoustic Waves Along Cylindrical Plasma Columns", A.Y. Wong (July 1965)*

R-2 "Stability Limits for Longitudinal Waves in Ion Beam-Plasma Interaction", B.D. Fried and A.Y. Wong (August 1965)*

R-3 "The Kinetic Equation for an Unstable Plasma in Parallel Electric and Magnetic Fields", B.D. Fried and S.L. Osakow (November 1965)†

R-4 "Low-Frequency Spatial Response of a Collisional Electron Plasma", B.D. Fried, A.N. Kaufman and D.L. Sachs (August 1965)†

R-5 "Effects of Collisions on Electrostatic Ion Cyclotron Waves", A.Y. Wong, D. Judd and F. Hai (December 1965)*

R-6 "Interaction Between Ion Beams and Plasmas", R. Rowberg, A.Y. Wong and J.M. Sellen (April 1966)*

R-7 "Observation of Cyclotron Echoes from a Highly Ionized Plasma", D.E. Kaplan and R.M. Hill (May 1966)*

R-8 "Excitation and Damping of Drift Waves", A.Y. Wong and R. Rowberg (July 1966)*

R-9 "The Guiding Center Approximation in Lowest Order", Alfredo Baños, Jr. (September 1966)†

R-10 "Plasma Streaming into a Magnetic Field", S.L. Ossakow (November 1966)†

R-11 "Cooperative Effects in Plasma Echo Phenomena", A.Y. Wong (March 1967)*

R-12 "A Quantum Mechanical Study of the Electron Gas Via the Test Particle Method", M.E. Rensink (March 1967)

R-13 "Linear and Nonlinear Theory of Grid Excitation of Low Frequency Waves in a Plasma", G.L. Johnston (April 1967)

R-14 "The Expansion and Diffusion of an Isolated Plasma Column", J. Hyman (May 1967)

R-15 "Two-pole Approximation for the Plasma Dispersion Function", B.D. Fried, C.L. Hedrick and J. McCune (August 1967)†

R-16 "Experimental Investigation of Electron Runaway Phenomena", J.S. DeGroot (August 1967)

R-17 "Parametric Coupling Between Drift Waves", F. Hai, R. Rowberg and A.Y. Wong (October 1967)*

R-18 "Cyclotron Echoes from Doppler Effects", A.Y. Wong (March 1968)

R-19 "Ion Wave Echoes", D.R. Baker, N.R. Ahern and A.Y. Wong (November 1967)*

R-20 "Cyclotron Echoes in Plasmas", D. Judd, Thesis (March 1968)

R-21 "Test Particle Theory for Quantum Plasmas", M.E. Rensink (October 1967)†

R-22 "Artificial Van Allen Belt", Charles F. Kennel (November 1967)

R-23 "Landau Damping of Ion Acoustic Waves in a Cesium Plasma with Variable Electron-Ion Temperature Ratio", K.B. Rajangam (October 1967)

R-24 "The Inhomogeneous Two-Stream Instability", G. Knorr (September 1967)

R-25 "Magnetic Turbulence in Shocks", C.F. Kennel and H.E. Petschek (December 1967)†

R-26 "Small Amplitude Waves in High Beta Plasmas", V. Formisano and C. Kennel (February 1968)†

R-27 "Low Beta Plasma Penetration Across a Magnetic Field", B.D. Fried and S. Ossakow (March 1968)†

R-28 "Annual Status Report", February 1, 1967-January 31, 1968, Principal Investigators A. Baños, Jr., B.D. Fried, C.F. Kennel

R-29 "The Theorist's Magnetosphere", C. Kennel (April 1968)

R-30 "Electromagnetic Pitch Angle Instabilities in Space", C.F. Kennel and F.L. Scarf (April 1968)†

R-31 "Electromagnetic Echoes in Collisionless Plasmas", A.Y. Wong (April 1968)*

R-32 "Parametric Excitation of Drift Waves in a Resistive Plasma", G. Weyl and M. Goldman (June 1968)†

R-33 "Parametric Excitation from Thermal Fluctuations at Plasma Drift Wave Frequencies", A.Y. Wong, M.V. Goldman, F. Hai, R. Rowberg (May 1968)*

R-34 "Current Decay in a Streaming Plasma Due to Weak Turbulence", S.L. Ossakow and B.D. Fried (June 1968)†

R-35 "Temperature Gradient Instabilities in Axisymmetric Systems", C.S. Liu (August 1968)†

R-36 "Electron Cyclotron Echo Phenomena in a Hot Collisionless Plasma", D. Judd (August 1968)

R-37 "Transverse Plasma Wave Echoes", B.D. Fried and Craig Olson (October 1968)†

R-38 "Low Frequency Interchange Instabilities of the Ring Current Belt", C.S. Liu (January 1969)†

R-39 "Drift Waves in the Linear Regime", R.E. Rowberg and A.Y. Wong (February 1969)*

R-40 "Parametric Mode-Mode Coupling Between Drift Waves in Plasmas", F. Hai and A.Y. Wong (January 1969)*

R-41 "Nonlinear Oscillatory Phenomena with Drift Waves in Plasmas", F. Hai and A.Y. Wong (September 1970)

R-42 "Ion-Burst Excited by a Grid in a Plasma", H. Ikezi and R.J. Taylor (February 1969)

R-43 "Measurements of Diffusion in Velocity Space from Ion-Ion Collisions", A. Wong and D. Baker (March 1969)*

R-44 "Nonlinear Excitation in the Ionosphere", A.Y. Wong (March 1969)

R-45 "Observation of First-Order Ion Energy Distribution in Ion Acoustic Waves," H. Ikezi and R. Taylor (March 1969)*

R-46 "A New Representative for the Conductivity Tensor of a Collisionless Plasma in a Magnetic Field", B.D. Fried and C. Hedrick (March 1969)†

R-47 "Direct Measurements of Linear Growth Rates and Nonlinear Saturation Coefficients", A.Y. Wong and F. Hai (April 1969)*

R-48 "Electron Precipitation Pulsations", F. Coroniti and C.F. Kennel (April 1969)†

R-49 "Auroral Micropulsation Instability", F. Coroniti and C.F. Kennel (May 1969)†

R-50 "Effect of Fokker-Planck Collisions on Plasma Wave Echoes", G. Johnston (June 1969)†

R-51 "Linear and Nonlinear Theory of Grid Excitation of Low Frequency Waves in a Plasma", G. Johnston (July 1969)

R-52 "Theory of Stability of Large Amplitude Periodic (BGK) Waves in Collisionless Plasmas", M.V. Goldman (June 1969)†

R-53 "Observation of Strong Ion Wave-Wave Interaction", R. Taylor and H. Ikezi (August 1969)

R-55 "Optical Mixing in a Magnetoactive Plasma", G. Weyl (August 1969)†

R-56 "Trapped Particles and Echoes", A.Y. Wong and R. Taylor (October 1969)*

R-57 "Formation and Interaction of Ion-Acoustic Solitons", H. Ikezi, R.J. Taylor and D.R. Baker (July 1970)*

R-58 "Observation of Collisionless Electrostatic Shocks", R. Taylor, D. Baker and H. Ikezi (December 1969)*

R-59 "Turbulent Loss of Ring Current Protons", J.M. Cornwall, F.V. Coroniti and R.M. Thorne (January 1970)†

R-60 "Efficient Modulation Coupling Between Electron and Ion Resonances in Magnetoactive Plasmas", A. Wong, D.R. Baker, N. Booth (December 1969)*

R-61 "Interaction of Quasi-Transverse and Quasi-Longitudinal Waves in an Inhomogeneous Vlasov Plasma", C.L. Hedrick (January 1970)

R-62 "Observation of Strong Ion-Acoustic Wave-Wave Interaction", R.J. Taylor and H. Ikezi (January 1970)

R-63 "Perturbed Ion Distributions in Ion Waves and Echoes", H. Ikezi and R. Taylor (January 1970)*

R-64 "Propagation of Ion Cyclotron Harmonic Wave", E.R. Ault and H. Ikezi (November 1970)

R-65 "The Analytic and Asymptotic Properties of the Plasma Dispersion Function", A. Baños, Jr. and G. Johnston (February 1970)

R-66 "Effect of Ion-Ion Collision and Ion Wave Turbulence on the Ion Wave Echo", Dan Baker (June 1970)

R-67 "Dispersion Discontinuities of Strong Collisionless Shocks", F.V. Coroniti (March 1970)†

R-68 "An Ion Cyclotron Instability", E.S. Weibel (April 1970)†

R-69 "Turbulence Structure of Finite-Beta Perpendicular Fast Shocks", F.V. Coroniti (April 1970)†

R-70 "Steepening of Ion Acoustic Waves and Formation of Collisionless Electrostatic Shocks", R. Taylor (April 1970)

R-71 "A Method of Studying Trapped Particles Behavior in Magnetic Geometries", C.S. Liu and A.Y. Wong (April 1970)*

R-72 "A Note on the Differential Equation $g'' + x^2 g = 0$", E.S. Weibel (April 1970)

R-73 "Plasma Response to a Step Electric Field Greater than the Critical Runaway Field, With and Without an Externally Applied Magnetic Field", J.E. Robin (June 1970)

R-74 "The UC Mathematical On-Line Systems as a Tool for Teaching Physics", B.D. Fried and R. White (August 1970)†

R-75 "High Frequency Hall Current Instability", K. Lee, C.F. Kennel, J.M. Kindel (August 1970)†

R-76 "Laminar Wave Train Structure of Collisionless Magnetic Slow Shocks", F.V. Coroniti (September 1970)†

R-77 "Field Aligned Current Instabilities in the Topside Ionosphere", J.M. Kindel and C.F. Kennel (August 1970)†

R-78 "Spatial Cyclotron Damping", Craig Olson (September 1970)

R-79 "Electromagnetic Plasma Wave Propagation Along a Magnetic Field", C.L. Olson (September 1970)†

R-80 "Electron Plasma Waves and Free-Streaming Electron Bursts", H. Ikezi, P.J. Barrett, R.B. White and A.Y. Wong (November 1970)*

R-81 "Relativistic Electron Precipitation During Magnetic Storm Main Phase", R.M. Thorne and C.F. Kennel (November 1970)†

R-82 "A Unified Theory of SAR Arc Formation at the Plasmapause", J.M. Cornwall, F.V. Coroniti and R.M. Thorne (November 1970)†

R-83 "Nonlinear Collisionless Interaction between Electron and Ion Modes in Inhomogeneous Magnetoactive Plasmas", N. Booth (December 1970)*

R-84 "Observations of Parametrically Excited Ion Acoustic Waves", R. Stenzel (March 1971)

R-85 "Remote Double Resonance Coupling of Radar Energy to Ionospheric Irregularities", C.F. Kennel (January 1971)†

R-86 "Ion Acoustic Waves in a Multi-Ion Plasma", B.D. Fried, R. White, T. Samec (January 1971)†

R-87 "Current-Driven Electrostatic and Electromagnetic Ion Cyclotron Instabilities", D.W. Forslund, C.F. Kennel, J. Kindel (February 1971)

R-88 "Locating the Magnetospheric Ring Current", C.F. Kennel and Richard Thorne (March 1971)

R-89 "Ion Acoustic Instabilities Due to Ions Streaming Across Magnetic Field", P.J. Barrett, R.J. Taylor (March 1971)

R-90 "Evolution of Turbulent Electronic Shocks", A.Y. Wong and R. Means (July 1971)*

R-91 "Density Step Production of Large Amplitude Collisionless Electrostatic Shocks and Solitons", David B. Cohen (June 1971)

R-92 "Turbulent Resistivity, Diffusion and Heating", B.D. Fried, C.F. Kennel, K. MacKenzie, F.V. Coroniti, J.M. Kindel, R. Stenzel, R.J. Taylor, R.B. White, A.Y. Wong, W. Bernstein, J.M. Sellen, Jr., D. Forslund and R.Z. Sagdeev (June 1971)

PPG-93 "Nonlinear Evolution and Saturation of an Unstable Electrostatic Wave", B.D. Fried, C.S. Liu, R.W. Means and R.Z. Sagdeev (August 1971)

PPG-94 "Cross-Field Current-Driven Ion Acoustic Instability", P.J. Barrett, B.D. Fried, C.F. Kennel, J.M. Sellen and R.J. Taylor (December 1971)

R-95 "3-D Velocity Space Diffsuion in Beam-Plasma Interaction without Magnetic Field", P.J. Barrett, D. Gresillon and A.Y. Wong (September 1971)

PPG-96 "Dayside Auroral Oval Plasma Density and Conductivity Enhancements due to Magnetosheath Electron Precipitation", C.F. Kennel and M.H. Rees (September 1971)

PPG-97 "Collisionless Wave-Particle Interactions Perpendicular to the Magnetic Field", A.Y. Wong, D.L. Jassby (September 1971)

PPG-98 "Magnetospheric Substorms", F.V. Coroniti and C.F. Kennel (September 1971)

PPG-99 "Magnetopause Motions, DP-2, and the Growth Phase of Magnetospheric Substorms", F.V. Coroniti and C.F. Kennel (September 1971)

PPG-100 "Structure of Ion Acoustic Solitons and Shock Waves in a Two-Component Plasma", R.B. White, B.D. Fried and F.V. Coroniti (September 1971)

PPG-101 "Solar Wind Interaction with Lunar Magnetic Field", G. Siscoe (Meteorology Dept.) and Bruce Goldstein (JPL) (November 1971)

PPG-102 "Changes in Magnetospheric Configuration During During Substorm Growth Phase", F.V. Coroniti and C.F. Kennel (November 1971)

PPG-103 "Trip Report - 1971 Kiev Conference on Plasma Theory and Visits to Lebedev and Kurchatov Institutes", B.D. Fried (October 1971)

PPG-104 "Pitch Angle Diffusion of Radiation Belt Electrons within the Plasmasphere", Lawrence R. Lyons, Richard M. Thorne, Charles F. Kennel (January 1972)

PPG-105 "Remote Feedback Stabilization of a High-Beta Plasma", Francis F. Chen, Daniel Jassby and M. Marhic (December 1971)

PPG-106 "Remote Plasma Control, Heating Measurements of Electron Distribution and Trapped Particles by Nonlinear Electromagnetic Interaction," A. Y. Wong, F. F. Chen, N. Booth, D. L. Jassby, R. Stenzel, D. Baker and C. S. Liu, June 1971

PPG-107 "Computational and Experimental Plasma Physics for Theoreticians," B. D. Fried, January 1972

PPG-108 "Threshold and Saturation of the Parametric Decay Instability," R. Stenzel and A. Y. Wong, November 1971*

PPG-109 "Laser Amplification in an Inhomogeneous Plasma," R. White, January, 1972

PPG-110 "External Production and Control of Electrojet Irregularities," K. Lee, P. K. Kaw and C. F. Kennel, January 1972†

PPG-111 "Ion Heating Via Turbulent Ion Acoustic Waves," R. J. Taylor and F. V. Coroniti, February 1972†

PPG-112 "Polarization of the Auroral Electrojet," F. V. Coroniti and C. F. Kennel, February†

PPG-113 "Mode Coupling and Wave Particle Interactions for Unstable Ion Acoustic Waves," Pablo Martin and Burton D. Fried, February 1972

PPG-114 "Parallel Magnetic Multi-pole Confinement of a Magnetic Field-Free Plasma," Thesis, Rudolph Limpaecher, March 1972

PPG-115 "Turbulence in electrostatic Collisionless Shock Waves," Robert Means, Thesis, April 1972

PPG-116 "Large Diameter, Quiescent Plasma in a Magnetospheric Field," Earl Ault, Thesis, April 1972

PPG-117 "Parasitic Pitch-Angle Diffusion of Radiation Belt Particles by Ion-Cyclotron Waves," L. R. Lyons and R. M. Thorne May 1972

PPG-118 "A New Role for Infrared Lasers," F. F. Chen, May 1972

PPG-119 "Electrostatic Instability of Ring Current Protons beyond the Plasmapause during Injection Events," F. V. Coroniti, R. W. Fredricks and R. B. White, May 1972

PPG-120 "Magnetospheres of the Outer Planets," C. F. Kennel, May 1972

PPG-121 "Measurement of Transverse and Longitudinal Heat Flow in a Laser-Heated, Magnetically Confined Arc Plasma," S. W. Fay, Thesis, June 1972

PPG-122 "Plasmaspheric Hiss," Richard M. Thorne, E. J. Smith, R. K. Burton, Robert E. Holzer, July 1972

PPG-123 "Magnetospheric Electrons,"F. V. Coroniti and R. M. Thorne, July 1972†

PPG-124 "Calculation of Reflection and Transmission Coefficients for a Class of One-Dimensional Wave Propagation Problems in Inhomogeneous Media," A. Baños, Jr., September 1972

PPG-125 "Electromagnetic Wave Functions for Parabolic Plasma Density Profiles," A. Baños, Jr. and D. L. Kelly, September 1972

PPG-126 "Amplification of Electromagnetic Waves in Overdense Plasmas," F. F. Chen and R. B. White, September 1972†

PPG-127 "Abstracts presented at the American Physical Society Division of Plasma Physics Annual Meeting, Monterey, November 13-16, 1972."

PPG-128 "Can the Ionosphere Regulate Magnetospheric Convection?" F. V. Coroniti and C. F. Kennel, October, 1972

PPG-129 "Nonlinear Stabilization of Oscillating Two-Stream Instability," K. Nishikawa, Y. C. Lee and P. K. Kaw, October 1972